

DEVELOPMENT OF BINARY AND TERNARY CHROMIUM,
ALUMINUM, CARBON THIN FILM COATINGS
FOR HOT CORROSION PREVENTION

by

Lik Ming Aw

A thesis submitted in partial fulfillment
of the requirements for the degree

of

Master of Science

in

Mechanical Engineering

MONTANA STATE UNIVERSITY
Bozeman, Montana

January 2015

©COPYRIGHT

by

Lik Ming, Aw

2015

All Rights Reserved

ACKNOWLEDGEMENTS

I would first like to thank my academic advisor and committee chair Dr. Roberta Amendola for providing me with such a wonderful opportunity to work on a research topic that I enjoyed throughout the entire process. I would also like to thank my committee members Dr. Paul Gannon and Dr. Stephen Sofie for their contribution and feedback during the research process to improve the quality of the study carried out. The completion of this particular thesis would not have been possible without the help, guidance, and support from Dr. Amendola, Dr. Gannon, and Dr. Sofie and I greatly appreciate their time and effort in this matter.

Apart from that, I would also like to thank the staff of the Imaging and Chemical Analysis Laboratory (ICAL) at Montana State University, Bozeman, especially Dr. Recep Avci, Laura Kellerman, Linda Loetterle, and Mark Wolfenden for their training and assistance in carrying out various materials characterization techniques that were essential in the analyses of data collected from experimentation. I would also like to thank Montana State University undergraduate and graduate students McLain Leonard, Grace Caldwell, John Ryter, Quinn Andrews, Josh Aller, and David Driscoll for their assistance in the research process.

Lastly, I would love to thank my family members from Malaysia and all my close friends and their families from all around the world for providing me with the love and support that helped provide me with the strength and willpower to complete this Master's thesis.

TABLE OF CONTENTS

1. INTRODUCTION	1
1.1 Materials for High Temperature Applications	1
1.2 Metals for High Temperature Applications	2
1.3 Project Motivation	5
2. BACKGROUND	6
2.1 Hot Corrosion	6
2.1.1 Mechanisms	6
2.1.2 Impacts of Hot Corrosion	12
2.2 Coatings for Hot Corrosion Prevention	15
2.2.1 High Temperature Protective Coatings	15
2.2.2 MAX Phase Coatings	17
2.2.3 Cr ₂ AlC Coatings	19
2.2.4 Binary Coatings for Thesis	20
2.3 Physical Vapor Deposition (PVD).....	20
2.3.1 Common PVD Techniques	20
2.3.2 Sputtering Processes	22
2.3.3 Types of Sputtering Systems	24
3. METHODOLOGY	30
3.1 Development of Thin Film Coatings	30
3.2 Exposure Testing of Samples	34
3.3 Materials Analysis	38
3.3.1 Gravimetric Analysis	39
3.3.2 Profilometry	39
3.3.3 Scanning Electron Microscopy	40
3.3.4 X-Ray Powder Diffraction Spectroscopy	41
3.3.5 X-Ray Photoelectron Spectroscopy	42
3.3.6 Metallographic Sample Preparation	44
4. RESULTS AND DISCUSSIONS	46
4.1 Target Deposition Rates.....	46
4.2 Thin Film Coating Characterization	47
4.3 Type II Hot Corrosion.....	56
4.3.1 Gravimetric Analysis (LTHC).....	56
4.3.2 XRD Results (LTHC).....	58
4.3.3 FEM and EDX (LTHC).....	63

TABLE OF CONTENTS CONTINUED

4.4 Type I Hot Corrosion	70
4.4.1 Gravimetric Analysis (HTHC)	70
4.4.2 XRD Results (HTHC)	74
4.4.3 FEM and EDX (HTHC)	75
5. CONCLUSION.....	81
BIBLIOGRAPHY	85

LIST OF TABLES

Table	Page
1. Equilibrium of p_{SO_3} Liquid Fuel Containing 0.5 wt% Sulphur	9
2. Preferred Protective Oxides for Prevention of various Reactions	17
3. Thermo-mechanical Properties of Cr_2AlC	19
4. Ni-201 Weight Percent Composition	30
5. Sputter Deposition Parameters for All Thin Film Coatings	33
6. Polishing Procedure Used for Metallographic Sample Preparation	45
7. Deposition Rates of Targets	46
8. Profilometry of Thicknesses of Each Thin Film Coating Material	47

LIST OF FIGURES

Figure	Page
1. Materials for High Temperature Applications	3
2. Hot Corrosion of Metals and Alloys	7
3. Effect of Temperature and Gas Composition to Corrosion Mechanisms	9
4. Initiation Stage and Propagation Stage of Hot Corrosion for IN-738 Alloy	11
5. Thermodynamic Stability Diagram of Na ₂ SO ₄ at Constant Temperature	12
6. Corrosion Rates of Pure Oxidation and Hot Corrosion	13
7. Type I Hot Corrosion in Aircraft Service Specimen	14
8. Type II Hot Corrosion for Marine Applications	14
9. Hot Corrosion of Platform and Blade Tip of Gas Turbines	15
10. 300µm Stamm Coating for Gas Turbine Blades	16
11. Crystal Structures of the Three MAX Phases	18
12. Schematic Diagram of Electron Beam Assisted Evaporation Chamber	21
13. Schematic Diagram of Pulsed Layer Deposition Chamber	22
14. Schematic Diagram of Sputtering Chamber	23
15. DC Sputtering System	25
16. RF Sputtering System	26
17. Magnetron Sputter Gun	28

LIST OF FIGURES CONTINUED

Figure	Page
18. Sputtering Source with Plasma	28
19. Racetrack Region of a Chromium Target in Magnetron Sputtering	29
20. Angstrom Magnetron Sputtering System for Thin Film PVD	31
21. MAK 3" Sputter Guns with Sputtering Targets Installed.....	32
22. Sartorius Model LE26P Balance for Mass Measurements.....	35
23. Ni-201 Samples Coated with 1 mgcm ⁻² Na ₂ SO ₄	36
24. Samples in Alumina Tube Crucibles for Exposure Testing.....	36
25. Schematic Diagram of Quartz Tube Setup	37
26. Ambios XP2 Computer Controlled Stylus Profilometer	40
27. Zeiss Spura 55VP Field Emission Scanning Electron Microscope.....	41
28. Scintag X1 Diffraction Spectrometer.....	42
29. X-Ray Photoelectron Spectrometer Physical Electronics 5600	43
30. Epoxy Sandwich Mounting Method for Sample Preparation	45
31. Sputter Deposited Samples before and after Heat Treatment.....	48
32. XRD Results of Al - C Deposition before and after Heat Treatment	49

LIST OF FIGURES CONTINUED

Figure	Page
33. XRD Results of Al - Cr Deposition before and after Heat Treatment	50
34. XRD Results of Cr - C Deposition before and after Heat Treatment	50
35. XRD Results of Cr - Al - C Deposition before and after Heat Treatment	51
36. XPS Survey for As Deposited Al – C and Heat Treated Al – C	53
37. XPS Survey for As Deposited Cr – Al and Heat Treated Cr - Al.....	54
38. XPS Survey for As Deposited Cr - C and Heat Treated Cr - C.....	54
39. XPS Survey for As Deposited Cr - Al - C and Heat Treated Cr - Al - C.....	55
40. Gravimetric Analysis of Type II Hot Corrosion.....	57
41. GIXRD Results for Uncoated Ni-201 after Type II Hot Corrosion Exposure.....	59
42. GIXRD Results for Al - C Coatings after Type II Hot Corrosion Exposure.....	59
43. GIXRD Results for Cr - Al Coatings after Type II Hot Corrosion Exposure.....	60
44. GIXRD Results for Cr - C Coatings after Type II Hot Corrosion Exposure.....	60
45. GIXRD Results for Cr-Al-C Coatings after Type II Hot Corrosion Exposure.....	61

LIST OF FIGURES CONTINUED

Figure	Page
46. Surface Morphologies before and after Type II Hot Corrosion Exposure of (a) Ni-201, (b) Al - C, (c) Cr - Al, (d) Cr - C, and (e) Cr - Al - C for 250 hours	64
47. Cross Sections with EDX Line Scans of (a) Ni-201, (b) Al - C, (c) Cr - Al, (d) Cr - C, and (e) Cr - Al - C Samples before Exposure	67
48. Cross Sections with EDX Line Scans of (a) Ni-201, (b) Al - C, (c) Cr - Al, (d) Cr - C, and (e) Cr - Al - C Samples after Type II Hot Corrosion Exposure for 250h.....	69
49. Gravimetric Analysis of Type I Hot Corrosion	71
50. (a) Samples after Type II Hot Corrosion Exposure for 250 hours, (b) Sample after Type I Hot Corrosion Exposure for 50 hours	73
51. GIXRD Results of Samples after Type I Hot Corrosion for 50 Hours	75
52. Surface Morphologies after Type I Hot Corrosion Exposure Testing of (a) Ni-201, (b) Al - C, (c) Cr - Al, (d) Cr - C, (e) Cr - Al - C Samples for 50 hours	76
53. Cross Sections with EDX Line Scans of (a) Ni-201, (b) Al - C, (c) Cr - Al, (d) Cr - C, and (e) Cr - Al - C Samples after Type I Hot Corrosion Exposure for 50 Hours	79

ABSTRACT

Increasing the operating temperature of high temperature energy conversion systems is often very desirable in order to maximize their corresponding efficiencies. Materials selected for high temperature applications must therefore incorporate associated considerations such as creep strength, high temperature corrosion resistance, and thermal fatigue.

Hot corrosion is a form of accelerated high temperature oxidation associated with the deposition of salt such as sodium sulfate (Na_2SO_4) on metals or their protective oxide surfaces. Severe corrosion develops when Na_2SO_4 reacts with metals to form eutectic (low-melting point) compositions on the surface of the metal at 700 °C (Type II Hot Corrosion) or when the surface has been wetted by molten Na_2SO_4 at 900 °C (Type I Hot Corrosion). This phenomenon reduces the useful life of materials such as nickel alloys used in high temperature gas turbines for aircraft and marine applications.

In this study, a variety of binary and ternary thin film coatings using chromium, aluminum, and carbon as base elements were deposited onto Ni-201 alloy and investigated as a function of exposure to hot corrosion environments. The coatings were deposited using a magnetron sputtering system and were approximately 1.5 μm in thickness. Prototypical Na_2SO_4 was applied to the samples before exposing them for up to 250 hours in an air/ SO_2 gas mixture at 700 °C and 900 °C, which simulates Type II and Type I Hot Corrosion, respectively.

It was determined that all coatings reduced the specific mass gains (corrosion rates) of the samples when compared to that of an uncoated sample, indicating that they provided protection against hot corrosion. For Type II Hot Corrosion, binary Cr – Al and ternary Cr – Al – C thin film coatings held up after 250 hours of exposure; whereas the other two coatings had completely disintegrated. For Type I Hot Corrosion, all thin film coatings utilized in the study had completely dissolved after 50 hours of exposure. It was suggested that the two most effective coating materials, Cr – Al and Cr – Al – C coatings should be used for future testing and that their thicknesses should be increased to help provide better protection against Type I Hot Corrosion.

CHAPTER ONE

INTRODUCTION

1.1 Materials for High Temperature Applications

One of the most important design considerations for systems utilized in major sectors of industry such as power generation, material processing, manufacturing, chemical engineering, transportation, and aerospace application are their operating temperatures (Meetham & Voorde, 2000). The majority of these systems run at high temperature and it is often strongly desirable to increase their respective operating temperatures as that would generally improve the possible thermodynamic efficiencies of these systems.

By increasing its firing temperature from 1316 °C to 1430 °C, 9H compressors developed by General Electric (GE) improved their thermal efficiency from 56% to 60% when compared to their previous 7F model (Matta, Mercer, & Tuthill, 2000), resulting in the first gas turbine combined-cycle system to achieve such thermal efficiency (Valenti, 2002). Another example of improved system efficiency with higher operating temperature is the design of military aircraft jet engines; higher operating temperature results in improved thrust to weight ratio of the aircraft while reducing fuel consumption (Meetham & Voorde, 2000).

The selection process of materials used in the design of high temperature systems is therefore of utmost importance; not only do the selected materials have to satisfy thermo-mechanical, chemical, electrical properties, along with cost effectiveness to

perform at elevated temperatures, they would also have to overcome other issues that may arise in high temperature environments such as creep, corrosion, and thermal fatigue.

Throughout this thesis, high temperature environments will always refer to operating temperatures of 500 °C and above. The selection of materials for high temperature applications depend considerably on the temperature regimes of operation. A list of materials used for high temperature applications with their corresponding operating temperature range is shown in Figure 1 (Ashby, Shercliff, & Cebon, 2010) to provide a better understanding of different families of materials typically selected within each temperature regime.

1.2 Metals for High Temperature Applications

Referring to the temperature regime of operation for different materials shown in Figure 1, refractory metals and ceramics are the primary candidates for applications above 1000 °C. This temperature regime exceeds the maximum service temperature of most metals and their alloys where they can reasonably be used without issues such as oxidation, chemical changes, and creep (Ashby, Shercliff, & Cebon, 2010).

However, metals and alloys are still main candidates for use in various fields at operating temperatures between 500 °C to 900 °C. Stainless steels, ferrous alloys, nickel-based alloys, and cobalt-based alloys satisfy the design requirements of typical systems operating within this temperature range such as steam turbines, gas turbine compressors, heat exchangers, and petrochemical reactors.

T °C	Materials	Applications	T K
1200	Refractory metals: Mo, W, Ta Alloys of Nb, Mo, W, Ta Ceramics: Oxides Al_2O_3 , MgO, etc. Nitrides, Si_3N_4 , Carbides, SiC	Rocket nozzles Special furnaces Experimental turbines	1400
1000			
800	Austenitic stainless steels Nichromes, nimonics Nickel based super-alloys Cobalt based super-alloys Iron based super-alloys	Gas turbines Chemical engineering Petrochemical reactors Furnace components Nuclear construction	1200
600			1000
400	Iron-based super-alloys Ferritic stainless steels Austenitic stainless steels Inconels and nimonics	Steam turbines Superheaters Heat exchangers	800
200	Low-alloy steels Titanium alloys (up to 450 °C) Inconels and nimonics	Heat exchangers Steam turbines Gas turbine compressors	600
0	Fibre-reinforced polymers Copper alloys (up to 400 °C) Nickel, monels and nickel-silvers PEEK, PEK, PI, PPD, PTFE and PES (up to 250 °C)	Food processing Automotive (engine)	400
-200	Most polymers (max temp: 60 to 150 °C) Magnesium alloys (up to 150 °C) Aluminum alloys (up to 150 °C) Monels and steels	Civil construction Household appliances Automotive Aerospace	200
-273	Austenitic stainless steels Aluminum alloys	Rocket casings, pipework, etc. Liquid O_2 or N_2 equipment	0
	Copper alloys Niobium alloys	Superconduction	

Figure 1. Materials for High Temperature Applications (Ashby, Shercliff, & Cebon, 2010)

One of the most favorable characteristics of metals is the diversity of manufacturing processes available to make and assemble components of complex shapes (Ashby, Shercliff, & Cebon, 2010). Within operating temperatures between 500 °C to 900 °C, the functional properties of metals can be manipulated and strengthened, which often involves some form of complementary mechanism to improve strength and environmental resistance to provide optimal performance and to prevent failure at high temperature (Meetham & Voorde, 2000; Ashby, Shercliff, & Cebon, 2010).

Nickel-based super-alloys have been developed to provide satisfactory creep rupture properties at 700 °C for up to 20,000 hours of operation in steam turbines (Ohno & Toji, 2007). Much research has also been carried out to develop specific ferritic stainless steels, chromium-based alloys, and nickel-based alloys to be used as interconnect materials for successful operation of solid oxide fuel cells at temperature ranges between 600 °C to 800 °C (Wang, Liu, & Fergus, 2011).

However, in some cases the strengthening methods alone might be inadequate for satisfactory performance of metallic materials in high temperature environments. When the overall design requirements for resistance to oxidation, corrosion, erosion, and wear cannot be satisfied by a single metallic material, additional processing is required to further improve the temperature capabilities of it. One of the most commonly used methods to provide resistance to these environments is the use of protective coatings; the inherent resistance of the base material is supplemented by the coatings, providing protection against harsh operating environment to ensure good performance and to achieve required component life (Meetham & Voorde, 2000).

1.3 Project Motivation

Carbide coatings have recently been developed for high temperature applications and it is of interest to further determine the effectiveness of Cr – Al – C coatings to improve the performance of nickel-based alloys in high temperature corrosive environments. The main objective of this thesis is to utilize the magnetron sputtering, a physical vapor deposition technique to deposit thin film ($< 5 \mu\text{m}$) binary and ternary Cr – Al – C coatings on nickel alloys to protect the base alloy against hot corrosion, a specific form of high temperature corrosion. Four different types of thin film protective coatings, namely chromium carbide (Cr_3C_2), aluminum carbide (Al_4C_3), chromium aluminum (AlCr_2), and chromium aluminum carbide (Cr_2AlC) were applied onto nickel 201 alloys before exposing the samples to various high temperature environments which simulated typical hot corrosive conditions in industrial applications of nickel-based alloys. The exposed samples were then further analyzed to evaluate the effectiveness and functionality of each coating material against hot corrosion.

In the next chapter, further description about hot corrosion environments, high temperature protective coatings, and thin film physical vapor deposition, will be presented to provide essential background information about the thesis before diving into more detail about the experiment, the results and the corresponding discussions.

CHAPTER TWO

BACKGROUND

2.1 Hot Corrosion

2.1.1 Mechanisms

Hot corrosion, also known as deposit-induced accelerated oxidation, is an aggressive mode of attack associated with the formation of salt deposits on the metal or oxide surface used in high temperature applications (Birks, Meier, & Pettit, 2006). This phenomenon occurs particularly in systems and components involved in the combustion products of fossil fuels, such as gas turbines used in combined cycle power plants and aircraft engines. Salt deposits resulting in hot corrosion generally include the sulfates, vanadates, and carbonates of sodium, calcium, and potassium (Pettit, 2011).

The most common deposit found in gas turbines is sodium sulfate (Na_2SO_4) where common salt (NaCl) in air or fuel react with sulfur existing as impurities in fuel to form Na_2SO_4 deposits on the base metal (Pettit, 2011). Na_2SO_4 will be the salt deposit analyzed in the thesis as it is the prototypical salt encountered in most real world applications and systems that are affected by hot corrosion.

A schematic diagram of the hot corrosion process is shown in Figure 2. Severe corrosion may develop when the surface of the metal has been wetted by a molten salt deposit as it influences the oxidation characteristics of it. In the absence of the deposits, protective oxide scales would form on the surface of the base metal, serving as a diffusion barrier to prevent further oxidation from occurring. However, molten Na_2SO_4

deposits undergo changes in composition at different environmental conditions which compromises the reaction-product barrier, resulting in the formation of non-protective scales that allow further degradation of the base metal (Birks, Meier, & Pettit, 2006).

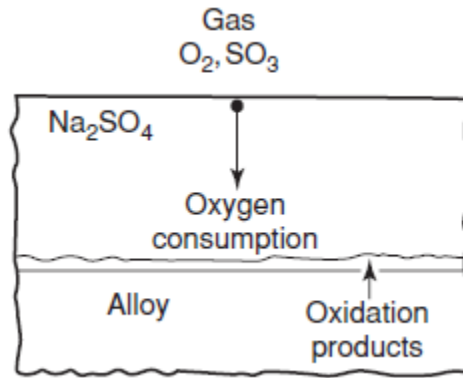
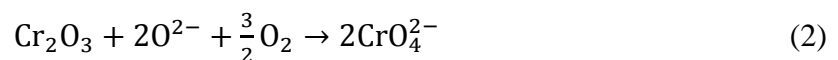


Figure 2. Hot Corrosion of Metals and Alloys (Birks, Meier, & Pettit, 2006)

Na_2SO_4 induced hot corrosion can be divided into two modes based on the temperature range in which accelerated oxidation occur. Type I Hot Corrosion, also known as high temperature hot corrosion (HTHC), is the active mode of degradation at temperatures above the melting point of Na_2SO_4 ($T_m = 884\text{ }^\circ\text{C}$), generally between $850\text{ }^\circ\text{C}$ to $950\text{ }^\circ\text{C}$ (Deodeshmukh & Gleeson, 2007). In this particular mode of hot corrosion, molten Na_2SO_4 wets the surface of the base material, resulting in the dissolution of thermally grown protective Al_2O_3 or Cr_2O_3 scales according to reactions (1) and (2) (Birks, Meier, & Pettit, 2006):



On the other hand, Type II Hot Corrosion (low temperature hot corrosion, LTHC) occurs at temperatures between $650\text{ }^\circ\text{C}$ to $750\text{ }^\circ\text{C}$ in the presence of sulfur trioxide. Low

temperature hot corrosion involves the reaction between solid salt and sulfates to result in the formation of a Na_2SO_4 - NiSO_4 eutectic which has a melting point well below that of pure Na_2SO_4 (Task, Gleeson, Pettit, & Meier, 2013). The NiSO_4 compound results from reaction (3) (Lillerud & Kofstad, 1984):



The relationship of different hot corrosion mechanisms as a function of temperature and SO_3 partial pressure is shown in Figure 3. This diagram is applicable to nickel and cobalt based alloys and it should provide a graphical representation of the conditions required to induce Type I Hot Corrosion and Type II Hot Corrosion in these systems.

The partial pressure of SO_3 (p_{SO_3}) play an important role in Type II Hot Corrosion as reaction (3) is greatly dependent upon it (Luthra & Shores, 1980). Referring to Figure 3 (Pettit, 2011), hot corrosion does not occur at 700 °C and low p_{SO_3} because Na_2SO_4 present in the system remains solid due to the lack of NiSO_4 in the system; as p_{SO_3} increases, Na_2SO_4 - NiSO_4 eutectic start forming and an abrupt increase in corrosion rate is experienced due to Type II Hot Corrosion.

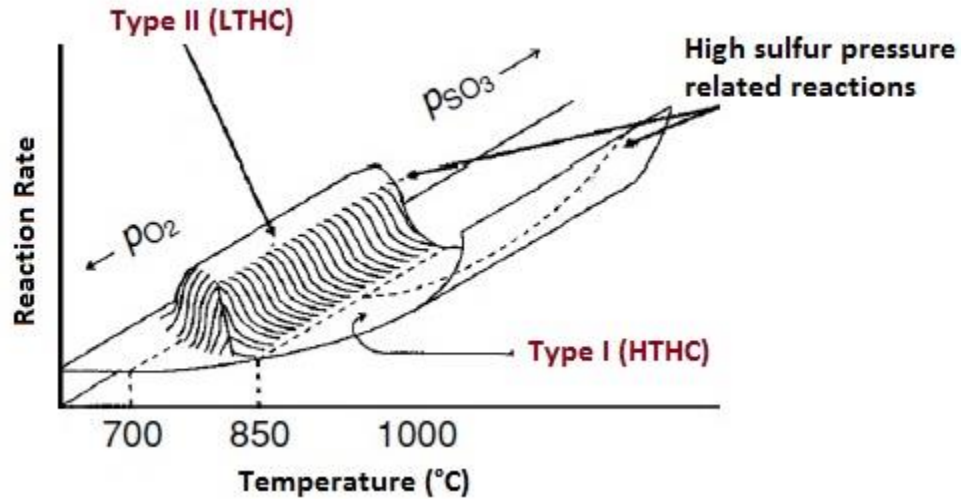


Figure 3. Effect of Temperature and Gas Composition to Corrosion Mechanisms (Birks, Meier, & Pettit, 2006)

The partial pressure of SO_3 is therefore a limiting factor of Type II Hot Corrosion; higher p_{SO_3} is required to enable the formation of NiSO_4 as temperature increases. However, the equilibrium SO_3 partial pressures in most combustion environments decrease as temperature increases (Table 1), resulting Type II Hot Corrosion to typically fall off at higher temperatures (Tschinkel, 1972). The reaction rate then experiences another spike as Type I Hot Corrosion, which is independent of p_{SO_3} , takes place at temperatures above 850 °C (Birks, Meier, & Pettit, 2006).

Table 1. Equilibrium of p_{SO_3} Liquid Fuel Containing 0.5 wt% Sulphur (Birks, Meier, & Pettit, 2006)

Temperature (K)	Equilibrium p_{SO_3} (atm)
700	7.5×10^{-4}
1100	3.8×10^{-4}
1400	9.8×10^{-5}

On the other hand, NiO required for the formation of NiSO₄ can be formed from the diffusion of Ni to the surface and the oxidation of Ni at elevated temperatures into NiO. Several studies have been carried out to examine the diffusion of Al – Cr – Ni systems (Pruthi, Anand, & Agarwala, 1977; Rothman, Nowicki, & Murch, 1980; Chen, Iijima, Hirano, & Kiyoshi, 1989; Debiaggi, Decorte, & Monti, 1996; Fujiwara & Horita, 2002; Allison & Samelson, 1958) and it was presented in all of them that considerable interdiffusion between Ni, Al, and Cr occurs at high temperatures. This provides a pathway for Ni diffusion through Al and Cr thin film coatings to the surface, allowing the formation of NiO which then reacts with SO₃ which then allows the formation of Type II Hot Corrosion inducing Na₂SO₄-NiSO₄ eutectic.

The hot corrosion of susceptible alloys occur in two stages: an initiation stage and a propagation stage. During the initiation stage, the rate of corrosion is slow and similar to that in the absence of salt deposit. The alloy and the deposit experience alterations such as the depletion of the protective scale, the incorporation of sulfur from the deposit into the alloy, and the development of cracks or channels in the scale which makes it vulnerable to rapid attack (Birks, Meier, & Pettit, 2006). The propagation stage then takes place when liquid deposit penetrates through the scale and is in contact with sections of the alloy depleted in Al or Cr, resulting in faster, sometimes catastrophic corrosion.

A plot of mass change against time for IN-738 alloy coated with 1 mgcm⁻² Na₂SO₄ in 1 atm O₂ is shown in Figure 4 (Birks, Meier, & Pettit, 2006) to illustrate the initiation stage and the propagation stage of hot corrosion. The dashed line in the figure gives an arbitrary measure of the end the initiation stage. A significant increase in weight

gain by the system is experienced past the dashed line, which is indicative of the propagation stage of hot corrosion in the IN-738 alloy.

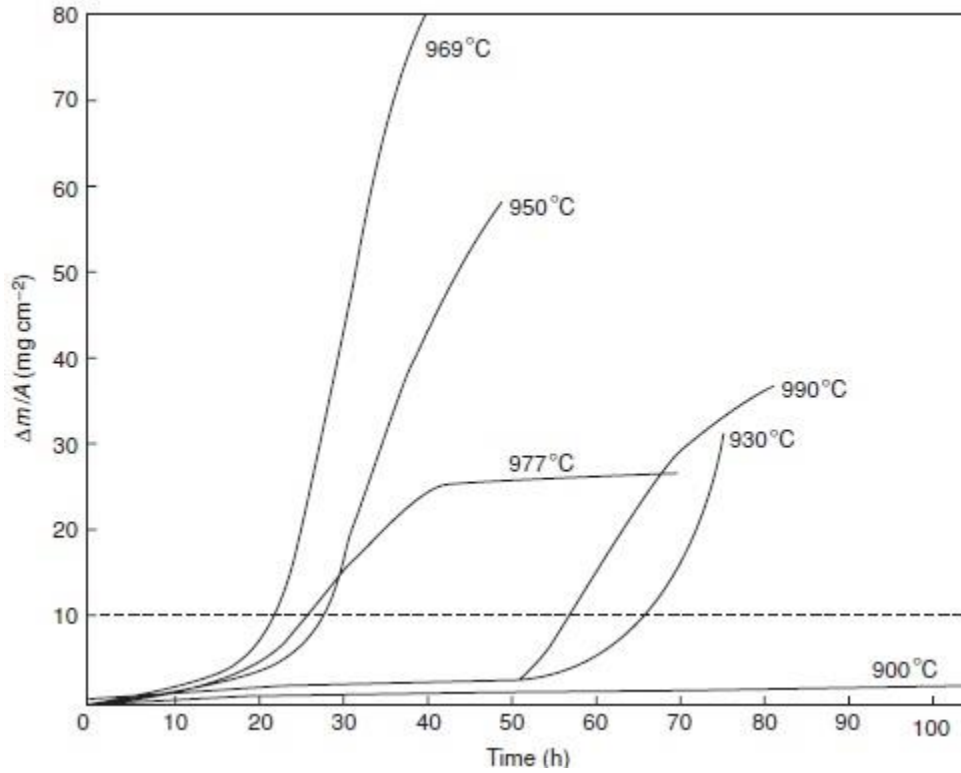


Figure 4. Initiation Stage and Propagation Stage of Hot Corrosion for IN-738 Alloy (Birks, Meier, & Pettit, 2006)

The composition of Na_2SO_4 at a given temperature during the initiation stage contributes greatly to hot corrosion as the prototypical salt deposit can become more basic or more acidic based on the oxygen partial pressure (p_{O_2}), and either by the activity of Na_2O , $a_{\text{Na}_2\text{O}}$, or the partial pressure of SO_3 (p_{SO_3}) (Birks, Meier, & Pettit, 2006) as depicted in Figure 5 and reaction (4).



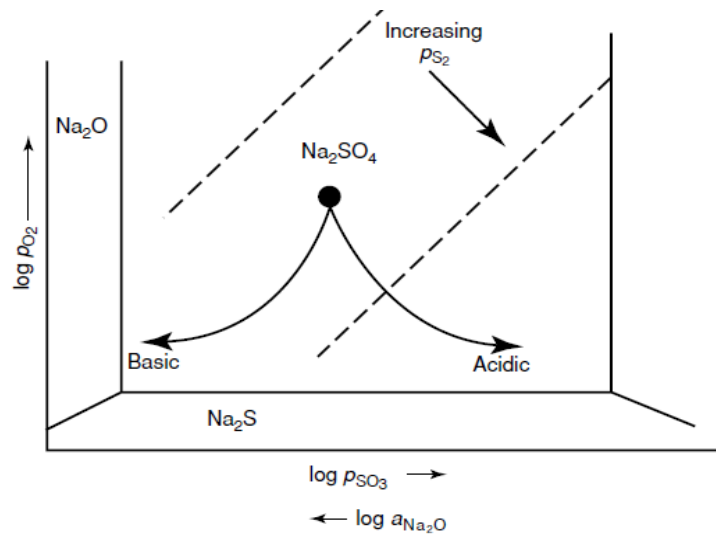


Figure 5. Thermodynamic Stability Diagram of Na_2SO_4 at Constant Temperature (Birks, Meier, & Pettit, 2006)

When Na_2SO_4 experiences a change in composition to become more acidic or more basic, it provides an environment where elements in the alloy are oxidized and electrons are transferred from metallic atoms to reducible species in the deposit. SO_3 or Na_2O in the Na_2SO_4 melt contributes to the oxygen ions (O^{2-}) necessary for reactions (1) and (2) to occur, dissolving any initially protective oxide layer on the surface of the alloy, which then results in the base metal to be exposed to further severe high temperature oxidation (Birks, Meier, & Pettit, 2006).

2.1.2 Impacts of Hot Corrosion

Hot corrosion is a serious issue to take into consideration during the design of high temperature systems dealing with the combustion products of fossil fuels. The rates of corrosion for pure oxidation and hot corrosion are shown in Figure 6 (Gleeson, 2013) to depict the detrimental effects of hot corrosion. Corrosion induced by Type I Hot Corrosion and Type II Hot Corrosion within their respective temperature range were

comparable to that of pure oxidation at significantly higher temperature, severely affecting the service life of the system, which in extreme cases can lead to failure.

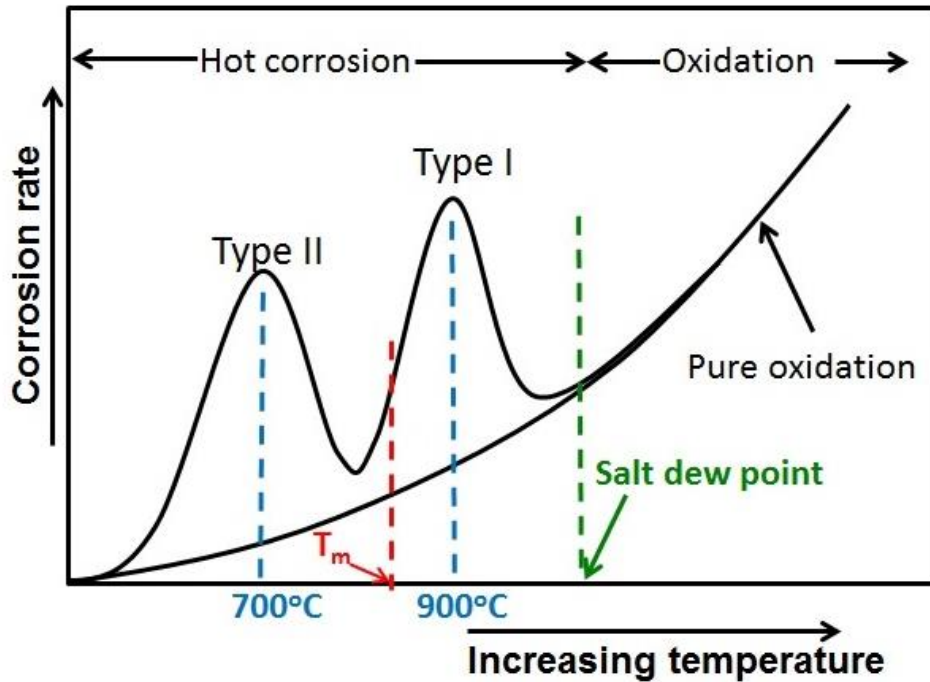


Figure 6. Corrosion Rates of Pure Oxidation and Hot Corrosion (Gleeson, 2013)

The earliest instance of hot corrosion was the accelerated wastage of stainless steel superheater supports in a marine boiler (Stringer, 1977). Materials used in advanced gas turbine engines have also been shown to experience Type I Hot Corrosion throughout the turbine airfoil section and Type II Hot Corrosion under the platform section of the airfoil (Deodeshmukh & Gleeson, 2007).

The microstructural features of Type I Hot Corrosion of an aluminide coated B-1900 nickel based superalloy used in aircraft service is shown in Figure 7 (Birks, Meier, & Pettit, 2006). Several spots of sulfide formation were detected when analyzing areas where the coating had been penetrated (Figure 7b and Figure 7c), showing that

sulfidation play an important role in the degradation of the superalloy. On the other hand, sulfidation or oxidation of Al and Cr were proposed as the operative degradation mechanism in Ni-based alloys for Type II Hot Corrosion (Figure 8) (Birks, Meier, & Pettit, 2006), which occurs in marine applications between 700 °C and 750 °C (Chiang, Pettit, & Meier, 1983; Barkalow & Pettit, 1978).

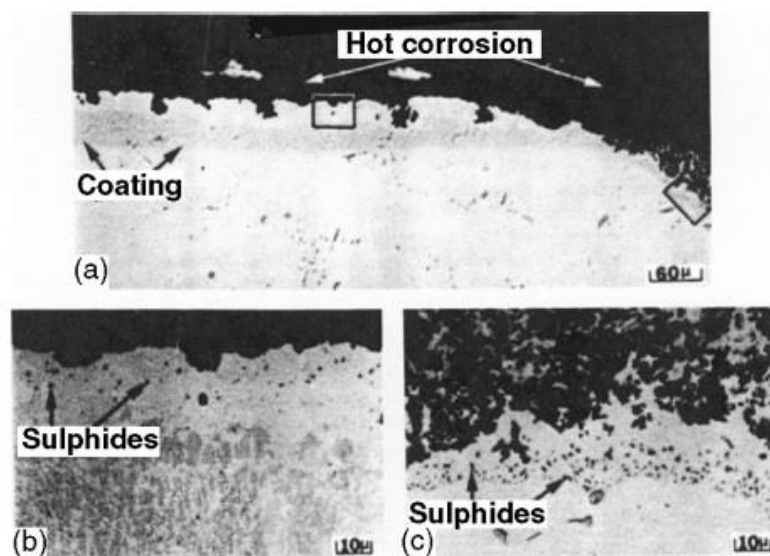


Figure 7. Type I Hot Corrosion in Aircraft Service Specimen (Birks, Meier, & Pettit, 2006)

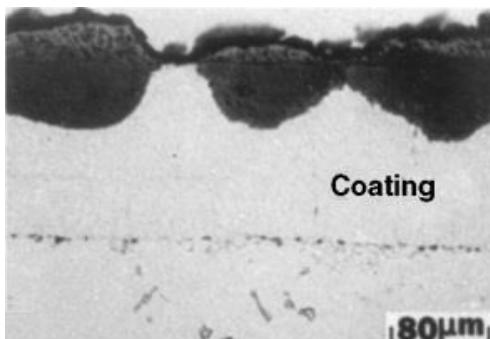


Figure 8. Type II Hot Corrosion for Marine Applications (Birks, Meier, & Pettit, 2006)

A combination of both Type I Hot Corrosion and Type II Hot Corrosion can also occur if their corresponding required conditions are met. A study on the failure of first

stage blades of a GE-F5 gas turbine indicated the presence of both types of hot corrosion on the blade tip and the platform (Khajavi & Shariat, 2004). The convex and concave sides of the platform were rough and had greenish appearance, while loss of material and thickness were observed on the top of the blade and green coloration on the concave side of the blade time (figure 9) (Khajavi & Shariat, 2004). The greenish color on the platform and blade tip have been reported as a macroscopic feature of Type I Hot Corrosion (Eliaz, Shemesh, & Latanision, 2002). It is also important to note that while both types of hot corrosion occurred in the study, Type I Hot Corrosion was dominant and that the gas turbine blade also suffered from erosion before failure (Kannan & Amirthagadeswaran, 2013).

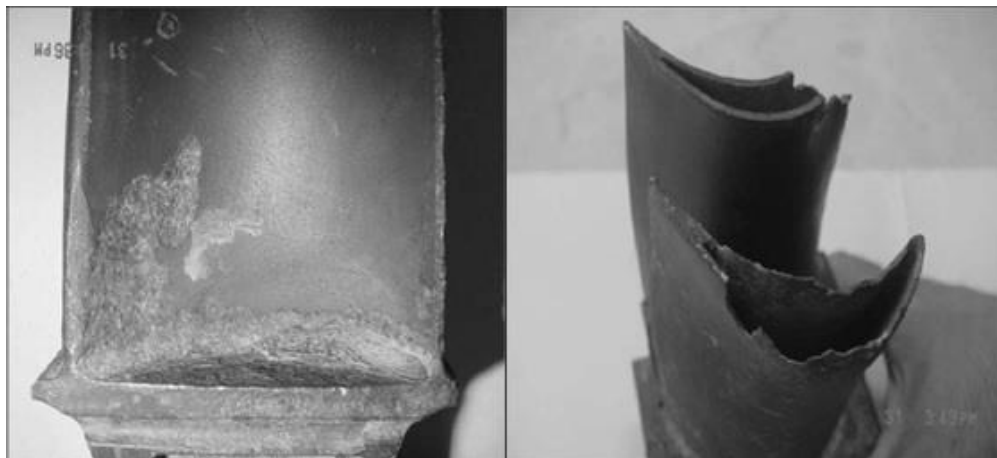


Figure 9. Hot Corrosion of Platform and Blade Tip of Gas Turbines (Kannan & Amirthagadeswaran, 2013)

2.2 Coatings for Hot Corrosion Prevention

2.2.1 High Temperature Protective Coatings

One of the most commonly implemented methods of hot corrosion prevention is the use of high temperature protective coatings on the surface of the alloy (Vargas, Ulion,

& Goebel, 1980). These coatings are designed to increase the life of the underlying alloy during service by forming continuous external oxide scales that have low growth rates and high temperature resistance (Sivakumar & Mordike, 1989). For example, a bond coating developed by Werner Stamm (Figure 10) at the Siemens Power Generation in Germany increased the service life of a nickel superalloy turbine blade from 4,000 hours to 25,000 hours with the help of protective aluminum oxide formation at high temperatures (Saini, 2012).



Figure 10. 300 μ m Stamm Coating for Gas Turbine Blades (Saini, 2012)

The composition of coating is typically selected to form oxide scales most effective in providing protection to the corresponding corrosive environment. A summary of the various corrosion processes encountered in practice along with the type of oxide that can offer resistance to that particular environment is provided in Table 2 (Sivakumar & Mordike, 1989).

Table 2. Preferred Protective Oxides for Prevention of Various Reactions (Sivakumar & Mordike, 1989)

Type	Reactant	Preferred Oxide	Applications
Oxidation	O ₂	Al ₂ O ₃ on Ni, Fe, or Co Alloys SiO ₂ on Refractory Alloys	Furnace Mufflers Heating Elements, Aircraft and Space Vehicle Components
Carburization	CO, CO ₂ , CH ₄	Al ₂ O ₃	Components in Petroleum Industry
Sulfidation	SO ₂	Cr ₂ O ₃	Coal Gassifiers
Hot Corrosion	Na ₂ SO ₄ , NaCl, V ₂ O ₅	Cr ₂ O ₃ , Al ₂ O ₃ , SiO ₂	Gas Turbine Blades, Vanes, Diesel Engine Components

It can be deduced from Table 2 that alumina (Al₂O₃) and chromia (Cr₂O₃) are the most suitable candidates for hot corrosion prevention; not only are they preferred in applications where hot corrosion is a problem, they also provide resistance to other forms of corrosion such as oxidation, carburization, and sulfidation. This piqued interest in using Cr₂AlC MAX phase coatings, which has been shown to form continuous alumina and chromia scale at high temperature (Li, Li, Xiang, Lu, & Zhou, 2011), as the thin film coating used for hot corrosion resistance in the thesis.

2.2.2 MAX Phase Coatings

MAX (abbreviation of M_{n+1}AX_n) phases are layered, hexagonal closed packed (HCP), early transition metal carbides and nitrides, where “M” is an early transition metal, “A” is a Group A element, typically from the IIIA or IVA Group, and “X” is either C or N (Barsoum, 2013). These compounds exhibit unique combination of metallic and ceramic properties. Similarly to metals, MAX phase compounds are damage tolerant,

electrically and thermally conductive, machinable, and thermal shock resistant. On the other hand, they exhibit characteristics indicative of ceramics, such as excellent thermal and chemical resistance, high elastic stiffness, and high melting point. The combination of desirable properties of metals and ceramics allowed these compounds to be potentially useful for high temperature structural components (Lee, Nguyen, & Park, 2012).

MAX phase compounds can be further divided into three groups depending on the number of layers of early transition metal (M layer) separating the Group IIIA or IVA element (A layer). In the 211 (M_2AX) phase, two M layers separate the A layer while three and four M layers exist between the A layer in the 312 (M_3AX_2) phase and the 413 (M_4AX_3) phase, respectively (Barsoum, 2013). The crystal structure of the 211, 312, and 413 phases are shown in Figure 11 (Hofsäss, 2007), where the M layers are colored in red, the A group elements in blue, and the X element in black.

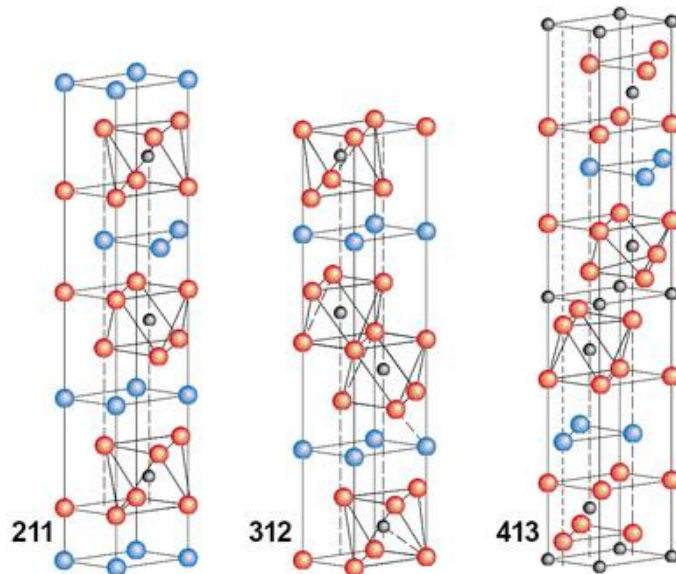


Figure 11. Crystal Structures of the Three MAX Phases (Hofsäss, 2007)

2.2.3 Cr₂AlC Coatings

Cr₂AlC is a ternary carbide which belongs to the 211 MAX phase group, where close packed layers of Cr are interleaved with layers of Al with C atoms filling the octahedral sites between the Cr layers (Lee, Nguyen, & Park, 2011). In addition to excellent thermo-mechanical properties (Table 3) (Tian, Wang, & Zhang, 2006), Cr₂AlC provides excellent oxidation resistance due to the formation of a thin protective oxides at high temperatures (Lee, Nguyen, & Park, 2012).

Table 3. Thermo-mechanical Properties of Cr₂AlC (Tian, Wang, & Zhang, 2006)

Coefficient of Thermal Expansion (α)	1.33 x 10 ⁻⁵ K ⁻¹
Thermal Conductivity at 200°C (k)	17.5 Wm ⁻¹ K ⁻¹
Vickers Hardness	3.5 GPa ~ 5.5 GPa
Young's Modulus (E)	278 GPa
Shear Modulus (G)	116 GPa
Melting Point (T_m)	1450 °C

The oxidation mechanism of Cr₂AlC coatings was described by Li et al. as follow: at the beginning of oxidation, aluminum in the coating reacts preferentially with oxygen to form a continuous layer of Al₂O₃ on the surface according to reaction (5) (Lin, Li, Wang, & Zhou, 2007). The consumption of aluminum in Cr₂AlC also results in partial transformation of the coating to Cr₇C₃, which starts to oxidize to form Cr₂O₃ according to reactions (6) and (7) when aluminum in the coating underneath the oxide scale becomes depleted (Li, Li, Xiang, Lu, & Zhou, 2011).



The formation of protective alumina layer on the surface of the coating was also observed in other studies with varying experimental parameters (Lee, Nguyen, & Park, 2012; Lee, Nguyen, & Park, 2011; Li, Li, Xiang, Lu, & Zhou, 2011; Lin, Li, Wang, & Zhou, 2007; Wang, et al., 2010; Wang, et al., 2010), however the coatings used in the studies had film thicknesses of more than 10 μm . It was therefore intriguing to determine if thin film ($< 5 \mu\text{m}$) Cr_2AlC coatings would exhibit similar hot corrosion resistance, which will be further examined in the thesis.

2.2.4 Binary Coatings for Thesis

Apart from carrying out experiments to determine the capabilities of thin film Cr_2AlC coatings for hot corrosion prevention, three other thin film binary coatings, chromium carbide, aluminum carbide, and chromium aluminum were also developed and exposed to the same corrosive environments to examine how they compare to their ternary (Cr_2AlC) MAX phase coatings.

2.3 Physical Vapor Deposition (PVD)

2.3.1 Common PVD Techniques

Physical vapor deposition (PVD) processes consist of technologies to deposit thin solid films through the condensation or nucleation of a vaporized form of the deposit, such as ions or plasma, to the surface of the substrate (Martin, 2011). In general, physical vapor deposition techniques consist of three fundamental steps: vaporization of the source material, transportation of the vapor to the surface of the substrate, and thin film deposition through vapor condensation (Sigma-Aldrich, 2014). These processes utilize a

line-of-sight method where the materials being deposited moves directly from the source to the substrate with little scatter, requiring PVD chambers to generally have low pressure during deposition to achieve such an effect (Martin, 2011).

Different physical mechanisms are implemented to generate the vaporized form of the deposit material in different PVD process. Evaporation process (Figure 12) (Hamdi & Ide-Ektessabi, 2003), which is one of the most commonly used PVD process, utilize resistive elements or high energy electron beams as heat sources to increase the temperature of the source to its corresponding vaporization temperature (Hamdi & Ide-Ektessabi, 2003). The vaporized particles of the source in the form of atoms or molecules then move from the source and adheres to the surface of the substrate over a wide range of angles with specific flux to ensure uniform distribution.

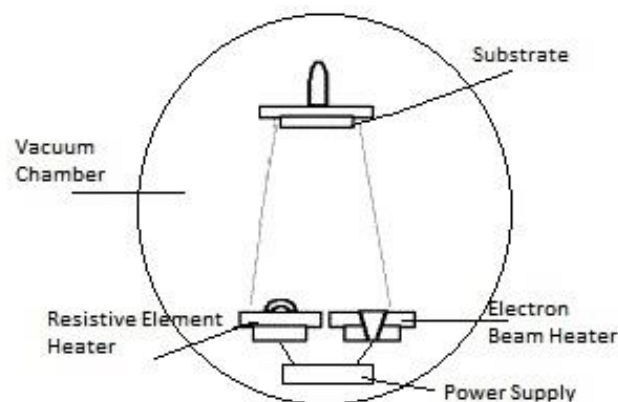


Figure 12. Schematic Diagram of Electron Beam Assisted Evaporation Chamber (Eason, 2007)

Another commonly used PVD technique for thin film deposition is pulsed laser deposition, where a pulsed laser beam is focused onto the target in a high vacuum chamber (Figure 13) (Eason, 2007). Each laser pulse vaporizes a small amount of the

material, creating a plasma plume, and is then ejected from the target in a forward-directed plume onto the substrate for film growth (Eason, 2007).

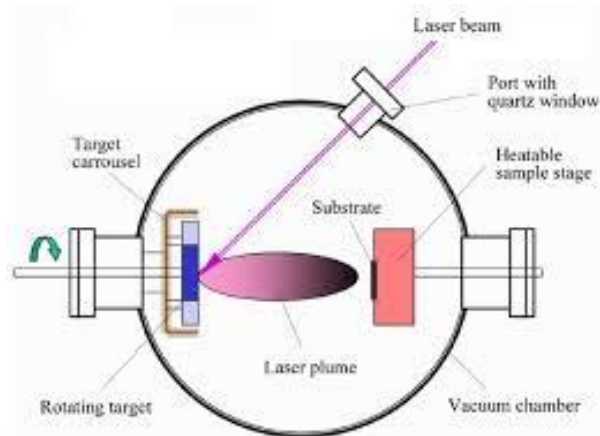


Figure 13. Schematic Diagram of Pulsed Layer Deposition Chamber (Eason, 2007)

Sputtering processes are also amongst the most commonly used PVD techniques. This particular family of PVD processes will be further discussed in the next section to allow better understanding about these systems as they were essential to the fabrication of thin film coatings for the experiments carried out in the thesis.

2.3.2 Sputtering Processes

When a solid or liquid at any temperature is subjected to bombardment of suitably high energy atomic particles, it is possible for individual atoms to acquire enough energy from the collision process to escape from the surface (Stuart, 1983). This means of causing ejection of atoms from a surface is called sputtering, and another family of widely used PVD systems utilize this phenomenon for the deposition of films.

Sputtering systems consist of a low pressure chamber where the sputtering source, also commonly referred to as the target, is bombarded by energetic gas ions until the

atoms or molecules of the target material gets ejected into a gas or plasma before depositing itself to the substrate (Martin, 2011). A schematic diagram of a simple sputtering chamber is shown in Figure 14 (Ohring, 1992); in this system argon gas ions are used as the energetic gas ions for the bombardment of the target in the sputtering chamber.

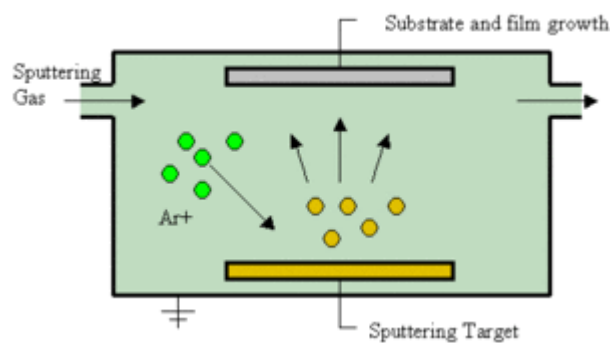


Figure 14. Schematic Diagram of Sputtering Chamber (Ohring, 1992)

The most distinctive advantage sputtering has over other PVD techniques is that thin films deposited using sputtering processes have properties and compositions close to that of the source, which is desirable in many thin film coatings applications (Martin, 2011). In contrast to the fractionation of alloy melts during evaporation due to rapid atomic diffusion and convection effects in the liquid phase, minimal solid state diffusion during the sputtering process enables the maintenance of the target and substrate composition (Ohring, 1992).

Sputtering is therefore widely used in the semiconductor industry for the deposition of metal alloy films of various materials for the manufacturing of integrated circuits. It is also an ideal method to deposit contact metals for thin film transistors due to

the low substrate temperature and good thin film properties obtainable during deposition (Fuller & Ghate, 1979).

Apart from that, sputtered atoms and molecules have higher kinetic energies during deposition, improving the adhesion of the films grown to the substrate when compared to that of evaporation (Martin, 2011). For example, the average ejection energy of germanium (Ge) atoms sputtered with 1.2 keV Ar⁺ ions is 15 eV, whereas that of evaporated germanium is only approximately 0.1 eV (Bunshaw, 1994). Both reactive and non-reactive processes can also be carried out and the use of multiple cathodes and reactive gases provides a straight forward way for the deposition of multilayer structures in sputtering systems (Martin, 2011).

2.3.3 Types of Sputtering Systems

Based on the difference in operating parameters and capabilities, sputtering processes can be divided into three categories: direct current (DC) sputtering, radio frequency (RF) sputtering, and magnetron sputtering. In DC sputtering systems (Figure 15) (Harsha, 2006), direct current power supplies are utilized to provide 0.5 kV to 5 kV of power to energize the electrodes in a vacuum chamber, where a glow discharge is produced and sustained by the electrons that are emitted and accelerated away from the target surface at energies equal to the cathode fall potential (Harsha, 2006). The primary electrons then enter the glow region and collide with the working gas atoms, causing the ionization of the gas which then results in the bombardment of the target surface to allow for sputter deposition (Harsha, 2006; Martin, 2011)

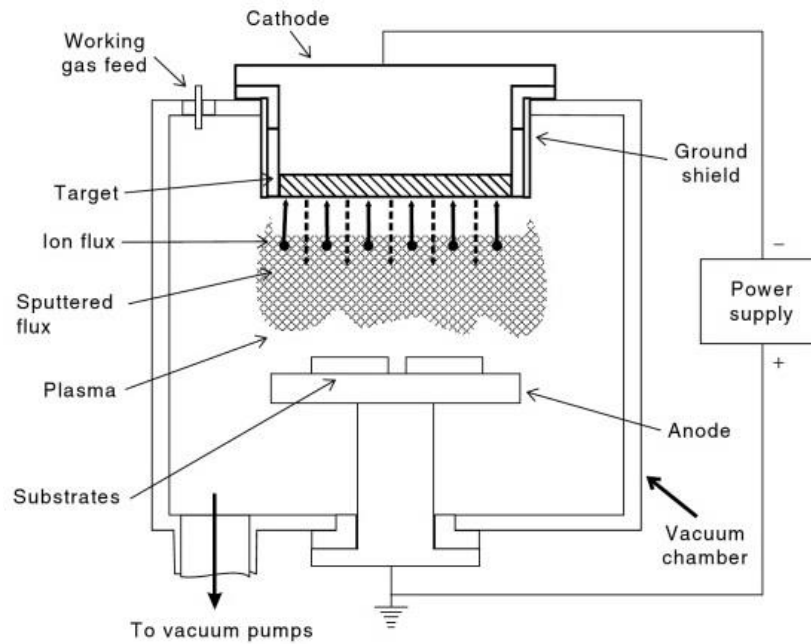


Figure 15. DC Sputtering System (Harsha, 2006)

However, DC sputtering can be used only for the thin film PVD of conductors as it is always necessary to apply a negative voltage to the target to sustain the glow discharge required for gas ionization; the use of RF sputtering (Figure 16) (Harsha, 2006) was then developed to allow the sputter deposition of nonconductive materials. By applying an alternating current signal with frequencies ranging from 5 MHz to 30 MHz to the electrode, electrons oscillating in the glow region acquire enough energy to cause ionizing collisions, reducing the need for secondary electrons to sustain the discharge. 13.56 MHz is conventionally used for RF sputtering due to the fact that it is the frequency reserved for plasma processing by the Federal Communications Commission (Ohring, 1992).

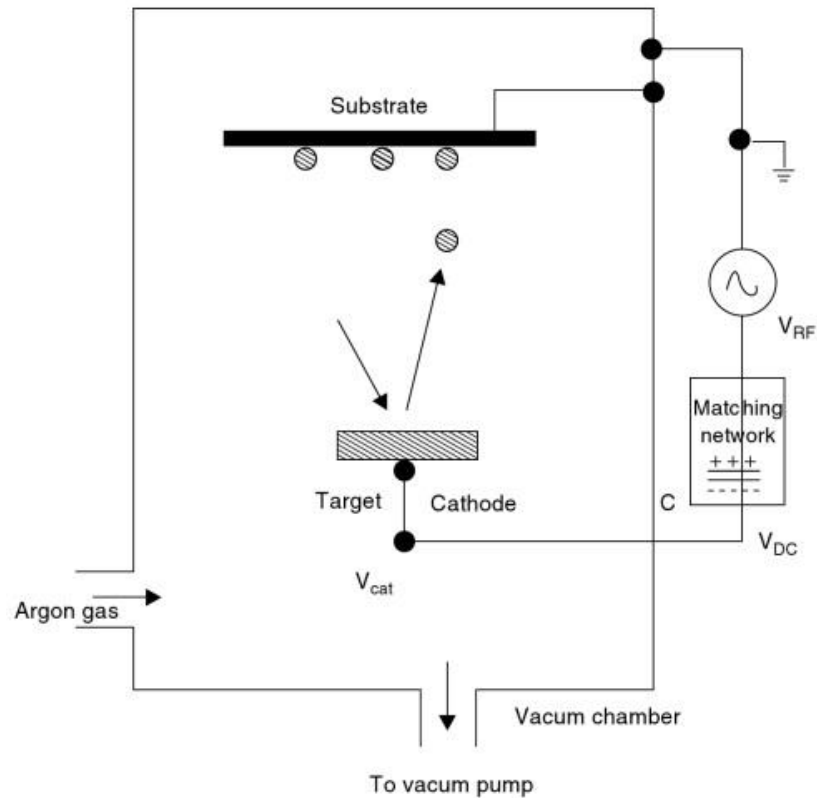


Figure 16. RF Sputtering System (Harsha, 2006)

While DC sputtering and RF sputtering enable the sputter deposition of a wide range of materials, limitations exist in each system that increased the need of a better system for sputter deposition. Apart from being unable to allow sputtering of nonconductive materials in DC sputtering systems, relatively high pressures (≈ 100 mTorr) are required to maintain the glow discharge in these systems, which changes the transportation of ejected atoms from a ballistic, line of sight transport to an undesirable diffusive transport (Harsha, 2006). Another common side effect of DC sputtering system is charge build-up on the target material due to large number of ions in the chamber (Walker, 2014).

On the other hand, while RF sputtering allows operation at lower pressure (< 15 mTorr) and the deposition of nonconductive materials, high rates of sputtering are limited by the ability of the target material to withstand thermal shock, and overheating of the target material is the most common issue with these systems (Walker, 2014; Harsha, 2006). In addition to that, the very low efficiency in the use of electrons to create ions in both DC sputtering and RF sputtering systems result in a deposition rate of less than $1000 \text{ \AA} \text{ min}^{-1}$ for metals and some hundreds of angstroms per minute for nonmetals (Harsha, 2006).

Increased ionization of the sputtering gas at a given pressure can come about by injecting additional electrons by thermionic or by field emission from an independent electrode, this resulted in the development of a more effective system for sputter deposition of thin films: the magnetron sputtering system (Harsha, 2006). In magnetron sputtering, both DC sputtering and RF sputtering can be utilized with the addition of magnetics under the targets in various configurations in the cathode enclosure (Martin, 2011). A magnetron sputter gun that uses a planar target and the plasma created during sputtering is shown in Figure 17 and Figure 18, respectively; when combining electric and magnetic fields in a magnetron sputtering chamber, the electrons remain in a trap near the target, confining the plasma to regions right above the target and increasing the ionizing effect of the working gas (Harsha, 2006; Martin, 2011).

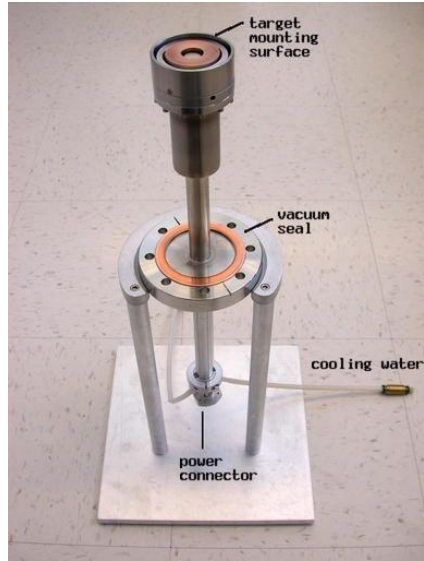


Figure 17. Magnetron Sputter Gun (Harsha, 2006)



Figure 18. Sputtering Source with Plasma (Harsha, 2006)

Magnetron sputtering systems can operate at pressure ranges significantly lower than that of conventional sputtering systems of 0.5 mTorr to 10 mTorr, which helps reduce the scattering and thermalization of sputtered particles with gas ion, improving the density and other properties of thin films deposited (Martin, 2011). Apart from that, the increased ionization of working gas greatly improves the deposition rates achievable with magnetron sputtering, making it the ideal thin film deposition process used for the protective coatings required for the thesis.

However, it is important to note that certain magnetron configurations suffer from low target material utilization. More sputtering of the target material occurs in a small region, often referred to as a “racetrack”, where the plasma concentration is at its highest due to the combination of the electric and magnetic fields. The racetrack region sputters preferentially whereas the rest of the target barely erodes, as shown in Figure 19 (Harsha, 2006).



Figure 19. Racetrack Region of a Chromium Target in Magnetron Sputtering

While the planar magnetron sputtering system utilized for the thin film PVD of protective coatings suffer from such drawbacks, it worked sufficiently for the scope of the thesis and was used successfully throughout the thin film PVD processes of the thin film protective coatings required for experimentation.

CHAPTER 3

METHODOLOGY

The objectives of the thesis were to develop thin film protective coatings using a magnetron sputtering system and to determine the effectiveness of each corresponding thin film coatings for hot corrosion prevention of nickel based alloys. Procedures carried out for the whole experiment process can be divided into three categories: development of thin film protective coatings, exposure testing of samples, and materials analysis.

3.1 Development of Thin Film Coatings

The thin film protective coatings desired for experimentation were deposited onto Ni-201 substrate which were donated to the high temperature materials laboratory and had been previously laser cut into 2 cm x 1 cm x 0.08 cm tabs. Ni-201 is a commercially available nickel and the ones used for this study consisted of compositions shown in Table 4. Using commercially available nickel Ni-201 for the experiments allow the fundamental analysis of the interaction between nickel and the various thin film coatings under hot corrosive environments.

Table 4. Ni-201 Weight Percent Composition (Allegheny Tech Inc., 2012)

Element	Fe	Si	Mn	Cu	C	S	Ni
Weight Percent (%)	0.05	0.05	0.02	0.02	0.02	0.002	Balance

The sputter deposition process was carried out using the Angstrom magnetron sputtering system provided by the Montana Microfabrication Facility (MMF) of Montana State University, Bozeman. The sputtering system (Figure 20) used was a load locked sputtering deposition system which had three MAK 3” sputter guns (two 1000 W RF and one 1000 W DC power supplies), enabling the simultaneous deposition of up to three targets (Himmer, 2011).



Figure 20. Angstrom Magnetron Sputtering System for Thin Film PVD

The three sputtering targets of interest, graphite (99.99% C), aluminum (99.999% Al), and chromium (99.99% Cr), were installed to the DC, RF1, and RF2 MAK 3” sputter guns, respectively, shown in Figure 21, and the sputtering chamber was pumped down to at least 1×10^{-7} Torr before carrying out any deposition process.

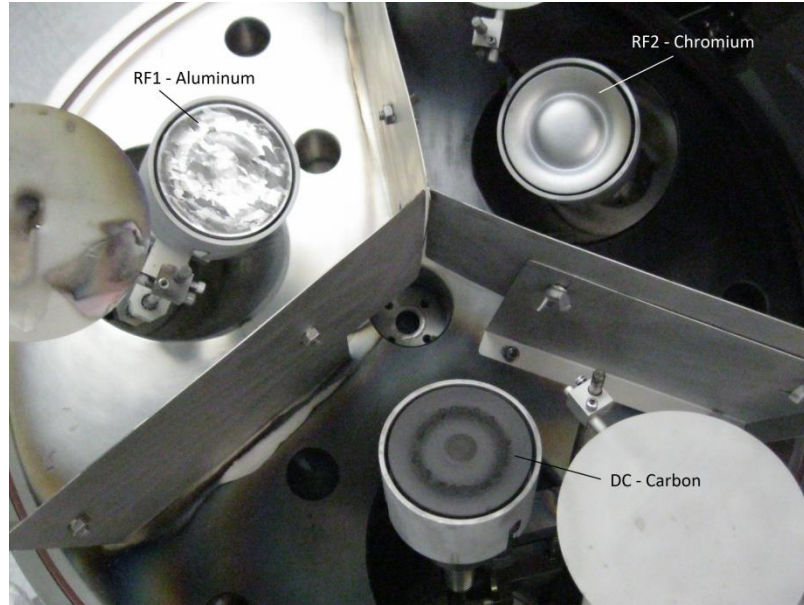


Figure 21. MAK 3" Sputter Guns with Sputtering Targets Installed

The deposition rates of each source at a stage height of 120 cm and chamber pressure of 5 mTorr were then determined by sputter depositing each element from 100 W to 500 W for 1 hour onto a glass slide; the resulting thicknesses were then measured with the Ambios XP2 computer controlled stylus profilometer from the Montana Microfabrication Facility. The deposition rates of each source at different power is presented in the next chapter.

The working recipe for the sputter deposition of each thin film coating was developed by manipulating the power of each target to achieve deposition rates closest to the stoichiometry of each desired coating. For example, during the deposition of Cr_3C_2 , the powers selected for the DC (C, 300 W) and the RF2 (Cr, 120 W) power supplies were chosen to result in a deposition rate of Cr: C of 125 nmh^{-1} : 80 nmh^{-1} , which corresponds to a stoichiometry of Cr: C of approximately 3: 2. The parameters used for each different thin film coating during magnetron sputtering deposition are shown in Table 5.

Table 5. Sputter Deposition Parameters for Thin Film Coatings

Parameter	Units	Al ₄ C ₃	Cr ₃ C ₂	AlCr ₂	Cr ₂ AlC
DC Power (C)	W	300	300	-	300
RF1 Power (Al)	W	120	-	250	100
RF2 Power (Cr)	W	-	120	200	150
Deposition Time	h	12	11	3.5	7
Stage Height	cm	120	120	120	120
Deposition Pressure	mTorr	5	5	5	5

The deposition times were selected to result in 1.5 μm of each coating from experimental values. A glass slide was attached to the sample holder and sputter deposited along with all other Ni-201 samples and the thickness of each coating was determined by using the Ambios XP2 profilometer upon completion of the sputter deposition process.

One coated sample from each set of deposition was taken out and analyzed using XPS and XRD from the ICAL to examine the characteristics of the samples directly after sputter deposition. The remaining samples were then heat treated at 500 °C for 1 hour in a low pressure furnace which was pumped down to 6×10^{-2} mTorr with a heating ramp rate of 5 °Cmin⁻¹.

The heat treated samples were then characterized using XPS and XRD to determine the coating composition before progressing on to the next phase of experimentation – the exposure testing of samples.

3.2 Exposure Testing of Samples

Upon completion of the sputter deposition of desired thin film coatings on Ni-201, the five sets of samples (uncoated Ni-201 and the 4 different thin film coated Ni-201) were then deposited with $1.0 \pm 0.3 \text{ mgcm}^{-2} \text{ Na}_2\text{SO}_4$ using a spray bottle deposition method before exposing them to simulated hot corrosive environments for testing.

$1 \text{ mgcm}^{-2} \text{ Na}_2\text{SO}_4$ was chosen as the specific mass (mass over surface area) of salt deposit for the thesis as it was the specific mass used in several other studies related to the hot corrosion resistance of nickel alloys and various thin film coatings (Gill, 2014; Birks, Meier, & Pettit, 2006; Ou, Sun, Sun, & Zou, 2008). Using the same specific mass of salt deposit enables the comparison of results obtained to that of the other studies.

The initial mass of each samples were measured using the Sartorius Model LE26P balance (Figure 22) which has an accuracy of $\pm 0.002 \text{ mg}$ (Sartorius Inc., 2014) and their corresponding desired mass after salt deposition recorded; the samples were then placed on a hot plate and heated up to $150 \text{ }^\circ\text{C}$ and a spray bottle containing 2% wt. Na_2SO_4 solution, calculated using equation (8) (Thompson, 2013), was used to spray the solution onto the surfaces of each samples to ensure even salt deposition. The samples were given ample time to dry off before spraying more Na_2SO_4 solution and they were also periodically weighed to check that the proper amount of salt was deposited.



Figure 22. Sartorius Model LE26P Balance for Mass Measurements

$$\text{Percent by Mass} = \frac{\text{Mass of Solute}}{\text{Mass of Solution}} \times 100\% \quad (8)$$

Once the desired deposit weight was achieved (Figure 23), each sample was stored in a desiccator for a day to remove any additional moisture. The salt deposited samples were then put inside alumina tube crucibles, shown in Figure 24, to help collect the scales which could spall during experimentation, which was a major source of error for the gravimetric analysis of previous studies (Gill, 2014). The total mass of samples with their alumina tube crucibles were recorded and used for the gravimetric analysis of the samples throughout the exposure testing.



Figure 23. Ni-201 Samples Coated with $1 \text{ mgcm}^{-2} \text{ Na}_2\text{SO}_4$



Figure 24. Samples in Alumina Tube Crucibles for Exposure Testing

The alumina tube crucibles were then placed in a quartz tube and a platinum mesh catalyst sandwiched between two quartz wool for support was slid to the inlet side and additional quartz wool was placed towards the outlet of the glass tube, as shown in Figure 25. The glass tubes were then inserted into one of the two tube furnaces in the high temperature materials laboratory to begin the exposure testing.

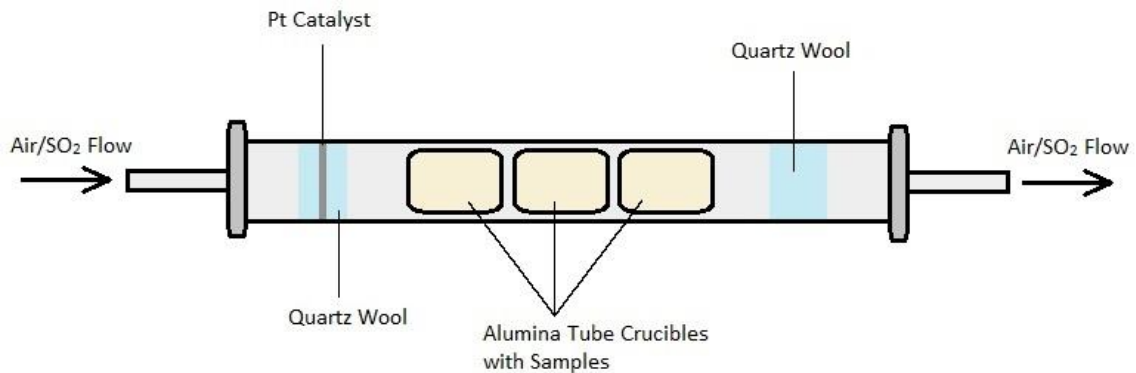


Figure 25. Schematic Diagram of Quartz Tube Setup

Both the MTI Corporation GSL1100X and Lindberg/Blue M TF55035A-1 tube furnaces were hooked up to a gas tank containing air/2 ppm SO₂ to provide the atmosphere required to induce hot corrosion. The platinum mesh at the inlet works as a catalyst increasing the conversion of SO₂ into SO₃ at high temperature; whereas the quartz wool placed at the outlet of the glass tube acts as a restrictor to promote turbulent flow and to provide additional thermal insulation within the quartz tube (Gill, 2014).

The samples (Ni-201, Al – C, Cr – Al, Cr – C, and Cr – Al – C) were exposed to the air/2ppm SO₂ atmosphere for a total of 250 hours at 700 °C to simulate Type II Hot Corrosion conditions. Gravimetric analysis was carried out using the Sartorius balance 1, 4, 10, 20, and 50 hour of exposure and in 50 hour increments after that; the collected data was used to produce a plot of mass gain per unit area over time for further analysis. The samples were heated up to 700 °C at a heating ramp rate of 10 °Cmin⁻¹ and the system was left to cool down for at least 3 hours after each desired exposure time before taking any mass measurements to prevent the spallation of salt deposits due to the temperature change.

After exposure testing and completing mass gain analysis of the samples at Type II hot corrosive environments, the samples were removed from their crucibles and washed in warm deionized water to remove any water soluble compounds. The surface morphologies and cross sections of all tested samples were then examined using the FESEM and EDX, while the phases present after Type II Hot Corrosion exposure were characterized using the XRD with thin film attachment at a grazing angle of 6° .

A new set of samples were then tested at Type I Hot Corrosion conditions; $1 \text{ mgcm}^{-2} \text{ Na}_2\text{SO}_4$ was deposited onto each sample before loading them up to the same air/2 ppm SO_2 glass tube fixture. The system was then heated up to 900°C and gravimetric analysis was carried out after 1, 4, 10 hour exposure and in 10 hour increments after that, to a final exposure time of 50 hours. The samples were then analyzed using the same materials characterization techniques as that of Type II Hot Corrosion exposed samples.

3.3 Materials Analysis

A combination of various materials analysis techniques including gravimetric analysis, profilometry, X-Ray Powder Diffraction (XRD), Field Emission Scanning Electron Microscopy (FESEM) with Energy Dispersive X-Ray Spectroscopy (EDX), and X-Ray Photoelectron Spectroscopy (XPS) were carried out during the experimentation process and in some cases, the findings from one materials analysis technique were crossed checked with other techniques to further reinforce the findings of the results.

3.3.1 Gravimetric Analysis

Gravimetric analysis is a technique in which the amount of a substance or chemical constituent of interest is quantified based on the mass measurements (Holler, Skoog, & West, 1996). During the exposure testing of the samples in hot corrosive environments, each sample undergoes an oxidation process and experiences an increase in mass based on the severity of oxidation. By measuring the mass of the samples before exposure and taking mass measurements at times specified in the previous section, the gravimetric analysis of each exposed sample allows the plot of change in specific mass gain (mass gain per unit area) over time, which indicates the severity of the hot corrosion process experienced by the sample.

The gravimetric analysis procedure of the samples has already been described in Section 3.2 using the Sartorius balance (Figure 22) and the findings are presented in the next chapter.

3.3.2 Profilometry

The thicknesses of each set of coatings were desired to be 1.5 μm and their corresponding thicknesses after deposition were determined using the Ambios XP2 computer controlled stylus profilometer (Figure 26) with a vertical resolution of 1 \AA (1×10^{-10} m) (Ambios Tech., 1996). The profilometer was also used to obtain the deposition rates of each sputtering targets at their respective power supplies at a sputtering height of 120 cm and chamber pressure of 5 mTorr, which was crucial in developing the working recipe for each thin film coating material of interest.

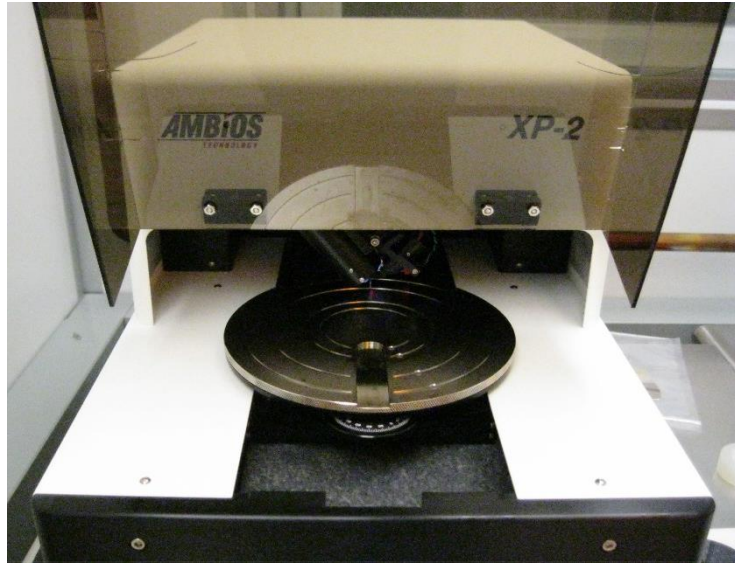


Figure 26. Ambios XP2 Computer Controlled Stylus Profilometer

3.3.3 Scanning Electron Microscopy

The surface morphologies and the cross sections of coated and uncoated samples, before and after exposure testing were examined and their corresponding images processed with the Zeiss Supra 55VP Field Emission Scanning Electron Microscope (Figure 27) from the ICAL. All surfaces of interest were imaged at a magnification of 1 kX or 10 kX with a working distance of 7 mm and a voltage of 5 kV, which were the parameters suggested by the ICAL personnel for good quality imaging.



Figure 27. Zeiss Spura 55VP Field Emission Scanning Electron Microscope

Spot scans and line scans of areas of interest have also been carried out using the energy dispersive x-ray spectroscopy (EDX), a system that has been built in the FESEM used. All x-ray spectra were collected at a magnification of 10 kX, a working distance of 15 mm and a voltage of 20 kV and their corresponding results are presented and discussed in the next chapter.

3.3.4 X-Ray Powder Diffraction Spectroscopy

The identification of the surface phases present all samples before and after exposure testing were carried out using the powder XRD method by observing the diffraction peaks attributed to the materials' crystal structure when x-rays are applied and

comparing them to powder diffraction data from the International Center for Diffraction Data (ICDD) (Zhang, Li, & Kumar, 2009).

The Scintag X1 Diffraction Spectrometer from the ICAL (Figure 28) was implemented to determine the phase compositions of sample surfaces before and after exposure testing. A thin film attachment was installed and a grazing incident angle of 6° was used for the analysis of surfaces of interest, as both additions help with the enhancement of information regarding the thin film regimes of interest.



Figure 28. Scintag X1 Diffraction Spectrometer

3.3.5 X-Ray Photoelectron Spectroscopy

The Physical Electronics 5600 X-ray Photoelectron Spectrometer (Figure 29) from the ICAL was utilized to characterize the elements presents on coated sample

surfaces before exposure testing. Samples loaded on the XPS was sputter cleaned with argon ions for 5 minutes before a survey from 0 eV to 800 eV was performed to obtain signals from all elements of interest in the experiments: carbon, chromium, aluminum, and oxygen.



Figure 29. X-Ray Photoelectron Spectrometer Physical Electronics 5600

This particular characterization technique allows not only the examination of the elemental composition of the surfaces tested, it also enables the identification of the chemical state of each element on the surface (Zhang, Li, & Kumar, 2009). For example, by looking at the binding energies of the carbon peaks in the survey, carbides ($E_b= 282$ eV) can be easily differentiated from elemental carbon and adventitious carbon ($E_b= 285$

eV). XPS analysis was only carried out on samples that have not been exposed to hot corrosion testing as samples after exposure testing consist of too many different phases with very similar binding energies, making this materials characterization technique not as effective as other methods such as the XRD.

3.3.6 Metallographic Sample Preparation

The cross sections of each set of samples before and after exposure testing were important to provide a visual representation of how effective each thin film coating serve as a diffusion barrier against severe oxidation due to hot corrosion. The metallographic sample preparation was performed before proceeding with further analysis using the Field Emission Microscope (FEM).

Samples after exposure testing that had Na_2SO_4 deposits were first washed with warm deionized water to remove the salt deposits. The samples were then sectioned using the Techcut 4 Precision Sectioning Machine and then attached to a polishing mount using an epoxy sandwich mount method, shown in Figure 30 (Gill, 2014). The samples were then grinded and polished with the TECHPREP Multiprep Polishing System according to the procedure used for polishing developed in collaboration with Allied High Tech, Inc., which is presented in Table 6.

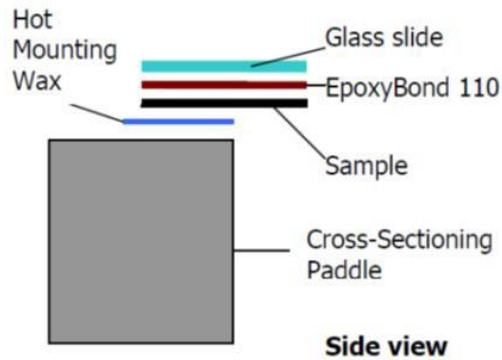


Figure 30. Epoxy Sandwich Mounting Method for Sample Preparation (Gill, 2014)

Table 6. Polishing Procedure Used for Metallographic Sample Preparation

Step	Grid Size	Type	Carrier	Coolant	Platen Speed (RPM)	Sample Load	Time
1	240 Grit	SiC	Abrasive Discs	Water	150/CCW	Full	As needed
2	480 Grit	SiC	Abrasive Discs	Water	150/CCW	Full	5 min
3	600 Grit	SiC	Abrasive Discs	Water	150/CCW	Full	5 min
4	800 Grit	SiC	Abrasive Discs	Water	150/CCW	Full	5 min
5	12 μm	Al_2O_3	Lapping Film	Red Lube	150/CCW	Full	5 min
6	9 μm	Al_2O_3	Lapping Film	Red Lube	150/CCW	Full	5 min
7	5 μm	Al_2O_3	Lapping Film	Red Lube	150/CCW	Full	5 min
8	3 μm	Al_2O_3	Lapping Film	Red Lube	150/CCW	Full	5 min
9	1 μm	Al_2O_3	Lapping Film	Red Lube	150/CCW	Full	5 min
10	0.3 μm	Al_2O_3	Microcloth	Suspension	150/CCW	Full	2-5 min

CHAPTER FOUR

RESULTS AND DISCUSSIONS

4.1 Target Deposition Rates

The determination of deposition rates for each target was performed as described in Section 3.1. While the initial plan was to determine the deposition rates for all three targets from 100 W to 500 W in 50 W increments, minor changes were made to more effectively determine the deposition rates of each sputtering source to develop the working recipe for the sputter deposition of desired thin film coatings.

The deposition rates for the magnetron sputtering of carbon proved to be the most difficult; not only were deposition rates too low and undetectable with the Ambios XP2 profilometer at powers ranging from 100 W to 200 W, the target fractured at powers above 300 W due to thermal shock. As a result, only a total of two data points were taken for the deposition rates of carbon (250 W and 300 W). The deposition rates of chromium and aluminum were then obtained from 100 W to 300 W at 50 W increments and presented in Table 7.

Table 7. Deposition Rates of Targets

Power (W) \ Source	Aluminum, RF1 (nmh⁻¹)	Chromium, RF2 (nmh⁻¹)	Carbon, DC (nmh⁻¹)
100	95	120	—
150	145	210	—
200	190	350	—
250	340	495	60
300	420	551	80

The limiting parameter for magnetron sputter deposition was having a maximum sputtering of carbon at 300 W, corresponding to a deposition rate of carbon of 80 nmh^{-1} ; the recipes for sputter deposition of thin films with carbon were then developed taking into account the maximum achievable deposition rate of carbon. Linear interpolation was used to decide the power at which chromium and aluminum should be sputtered at to obtain the desired coating stoichiometry (Al_4C_3 , AlCr_2 , Cr_3C_2 , and Cr_2AlC), which has been generally used in practice while working with magnetron sputtering systems (Himmer, 2011). The finalized working recipe executed for the magnetron sputtering of thin films on Ni-201 can be referred back to in Table 5 (Section 3.1).

4.2 Thin Film Coating Characterization

The thicknesses of each deposited thin films were measured using the profilometer and presented in Table 8. All coatings had thicknesses of $1.5 \pm 0.3 \text{ }\mu\text{m}$, which were within similar enough for the analysis required to determine their corresponding capabilities against hot corrosion, as the thin film coatings provided very consistent results during the exposure testing of them, which will be presented later in this chapter.

Table 8. Profilometry of Thicknesses of Each Thin Film Coating Material

Coating Type	Coating Thickness (μm)
Al – C	1.5
Cr – Al	1.4
Cr – C	1.7
Al – Cr – C	1.8

The next step was to check if thin films deposited contained desired chemical compounds desired (Al_4C_3 , AlCr_2 , Cr_3C_2 , and Cr_2AlC). Heat treatment of each set of sputter deposited samples was done directly after magnetron sputter deposition, at a low pressure furnace (6×10^{-2} mTorr) at 500°C for 1 hour to aid the formation of necessary crystalline structures and the samples before and after heat treatment is shown in Figure 31.

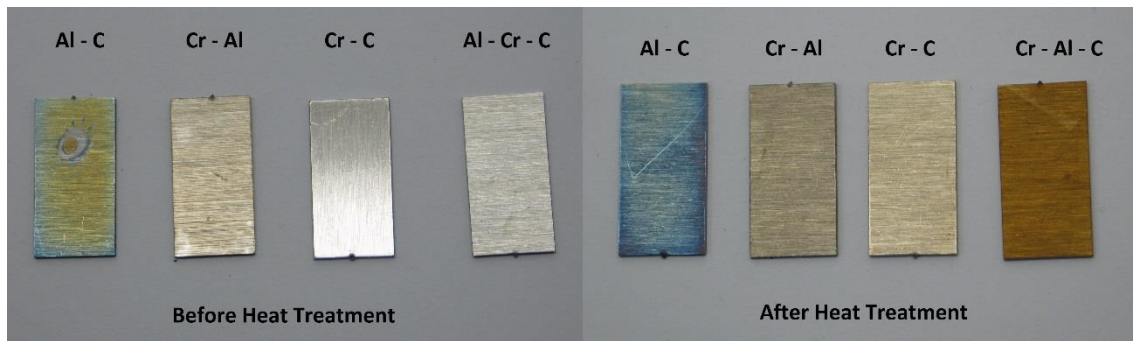


Figure 31. Sputter Deposited Samples before and after Heat Treatment

Visual comparison of coated samples before and after heat treatment suggests that this process induced a change that may be related to the transformation from an amorphous structure to a crystalline structure in the Cr - C and Cr - Al - C deposited thin films, as both those samples experienced a change in their respective coating colors. Structured layers of thin films have been known to alter the way light transmits and reflects due to thin film interference, allowing thin films to exhibit various colors (Knittl, 1978). It can also be deduced that the Al - C deposited samples showed some degree of crystallinity before undergoing heat treatment due to the colors they exhibit directly after sputter deposition.

The heat treated samples were then characterized using XRD and XPS and were compared with samples that were not heat treated. Figures 32 to 35 show the XRD results of the four magnetron sputtering deposited coatings (Al – C, Cr – Al, Cr – C, and Al – Cr – C) before and after heat treatment. In general, the heat treating process allowed all coated samples to reach their respective crystalline structures as exhibited by the distinct peaks observed in grazing incident XRD (GIXRD) results.

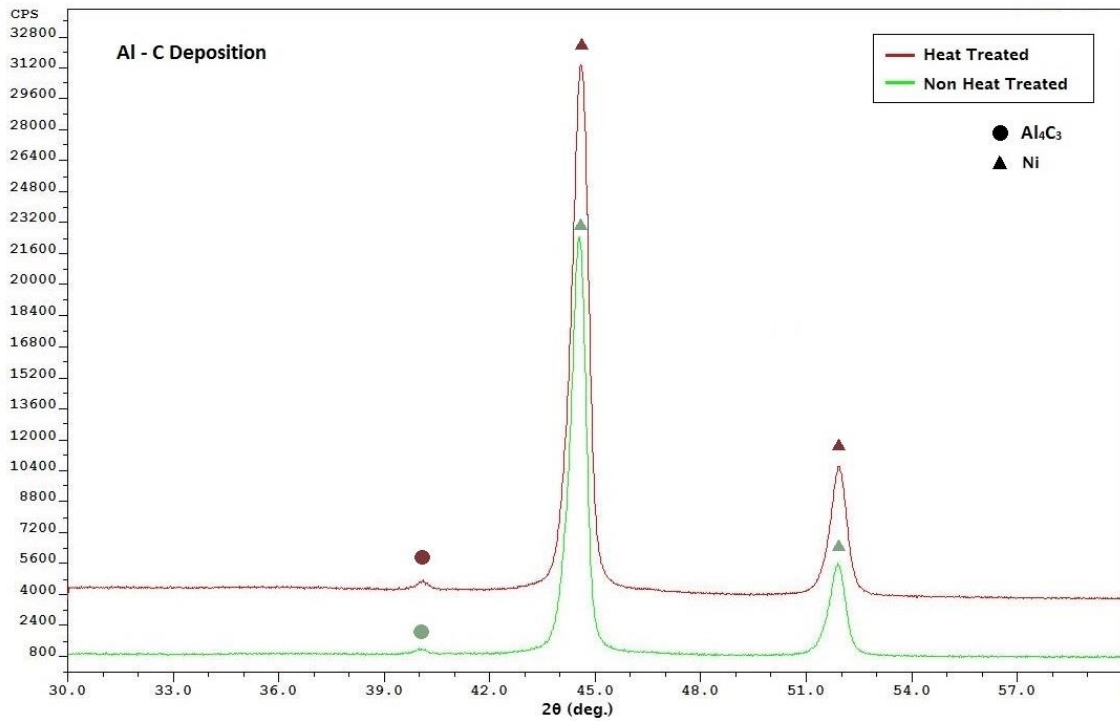


Figure 32. XRD Results of Al - C Deposition before and after Heat Treatment

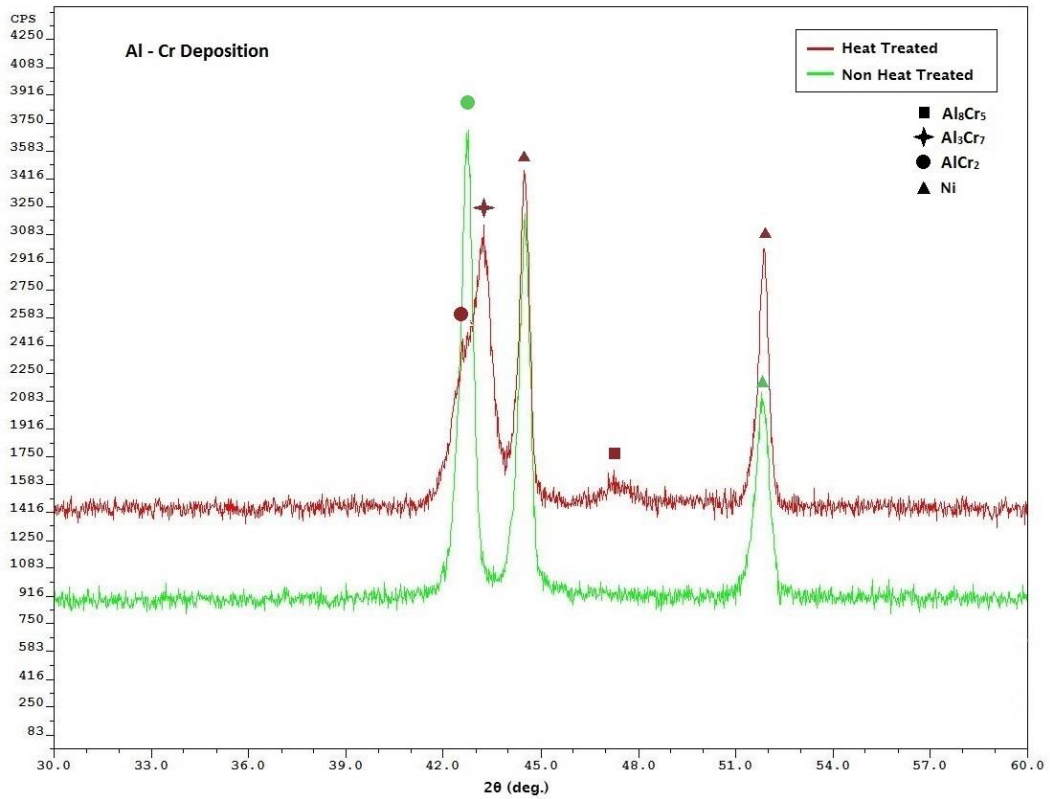


Figure 33. XRD Results of Cr - Al Deposition before and after Heat Treatment

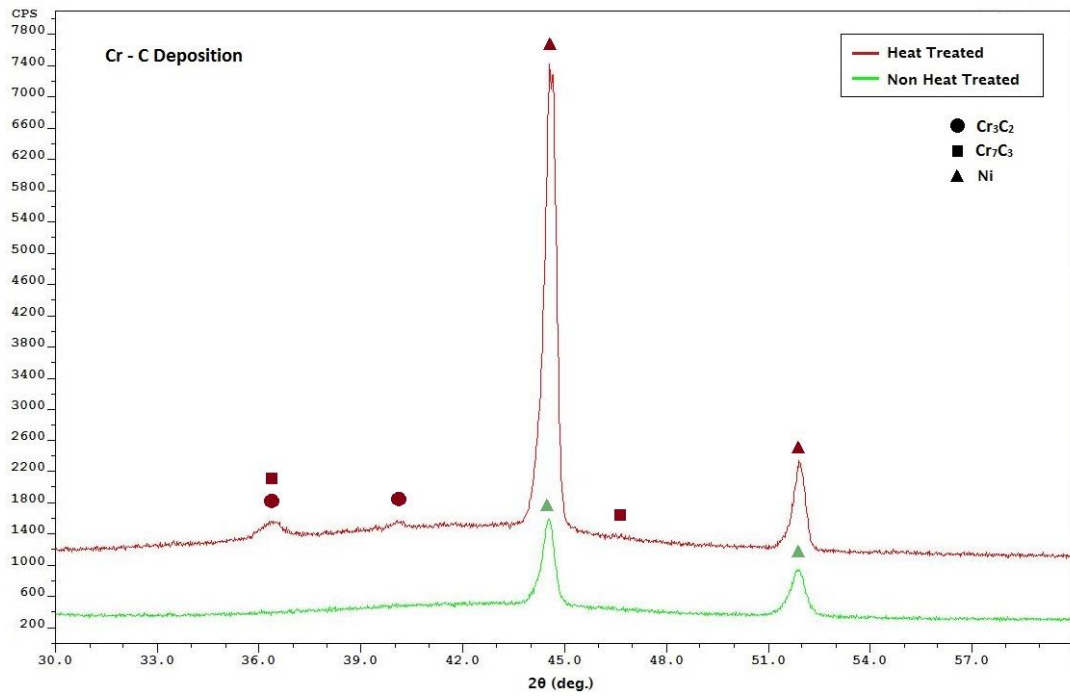


Figure 34. XRD Results of Cr - C Deposition before and after Heat Treatment

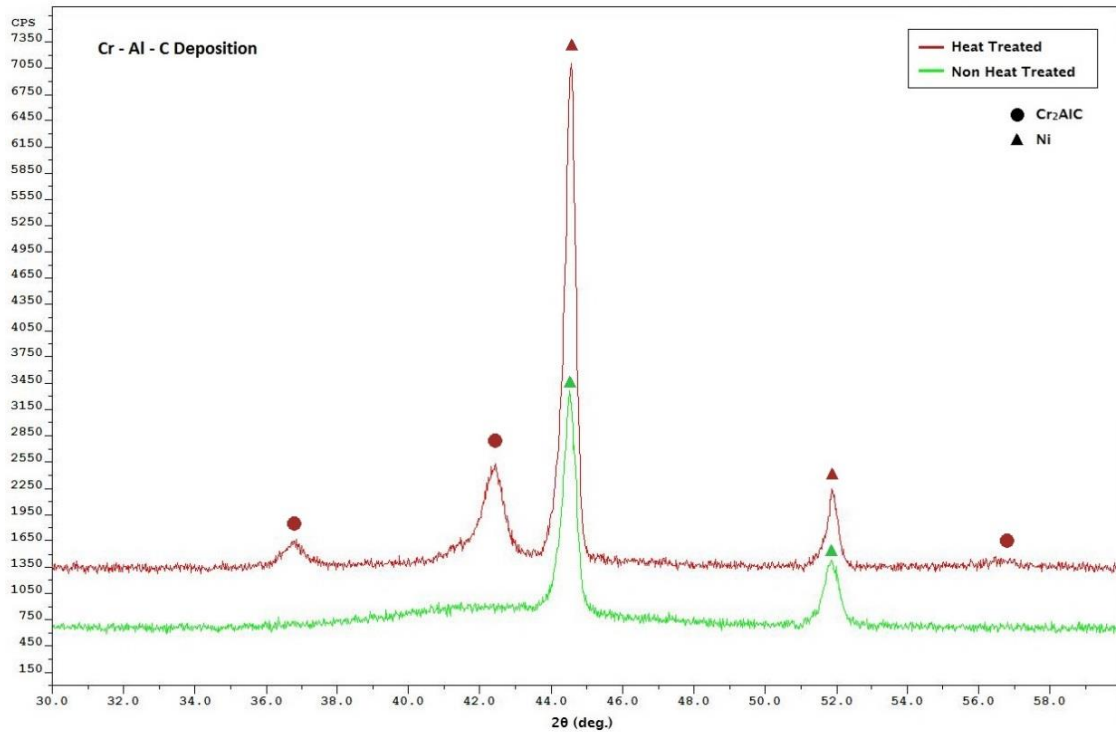


Figure 35. XRD Results of Cr - Al - C Deposition before and after Heat Treatment

A study by Yari et. al. indicated that magnetron sputtered carbon coatings that were deposited at low substrate temperatures of 100 °C and 200 °C were completely amorphous. By increasing the substrate temperatures to above 400 °C the structure of carbon films becomes glassy and nano-structural (Yari, Larijani, Afshar, Eshghabadi, & Shokouhy, 2012), which was the same with GIXRD results of heat treated thin film carbide coated samples deposited in this thesis.

This change from an amorphous structure to a crystalline structure was especially evident in the Cr - C and Cr – Al – C deposited thin films (Figure 34 and Figure 35). Before heat treatment, GIXRD results showed no peaks indicating the presence of any desired phases; whereas crystalline Cr_3C_2 and Cr_7C_3 in the Cr – C coated samples and

Cr_2AlC in the Cr – Al – C coated samples were identified in the samples after heat treatment.

As predicted from visual observation of Al – C coated samples, GIXRD results (Figure 32) showed Al_4C_3 peaks before heat treatment, indicating the preferential formation of crystalline Al_4C_3 at low substrate temperatures. However, heat treatment could have also assisted with the formation of crystalline Al_4C_3 . This was hypothesized based on not only in the higher intensity of Al_4C_3 peaks detected in GIXRD, but also from visual observation of the more evenly distributed bluish tint in heat treated Al_4C_3 (Figure 31).

On the other hand, GIXRD results for Cr - Al deposition (Figure 33) showed crystalline structures in both non heat treated and heat treated samples. It was determined from that at low deposition temperatures, AlCr_2 was the dominant crystalline phase present; samples after heat treatment showed combinations of various chromium aluminum compounds (AlCr_2 , Al_8Cr_5 and Al_3Cr_7) at elevated temperatures.

Based on the research work of others regarding the study of Al - Cr systems, AlCr_2 , Al_8Cr_5 , and Al_3Cr_7 are intermediate phases, in which only AlCr_2 forms congruently and the rest are formed by a series of peritectic reactions (Liang, Guo, Li, & Du, 2007; Murray, 1998; Koster, Watchtelund, & Grube, 1963), explaining the preferential formation of AlCr_2 at low substrate temperatures. Heat treatment of this particular thin film coating provided a mean to allow the formation of intermediate chromium aluminum compounds on the surface of the samples.

On the other hand, results from x-ray photoelectron spectroscopy (XPS) allowed the understanding of elemental compositions and the chemical state of each constituting elements on the samples' surface. Figures 36 to 39 presents the XPS results for all depositions completed with the magnetron sputtering system.

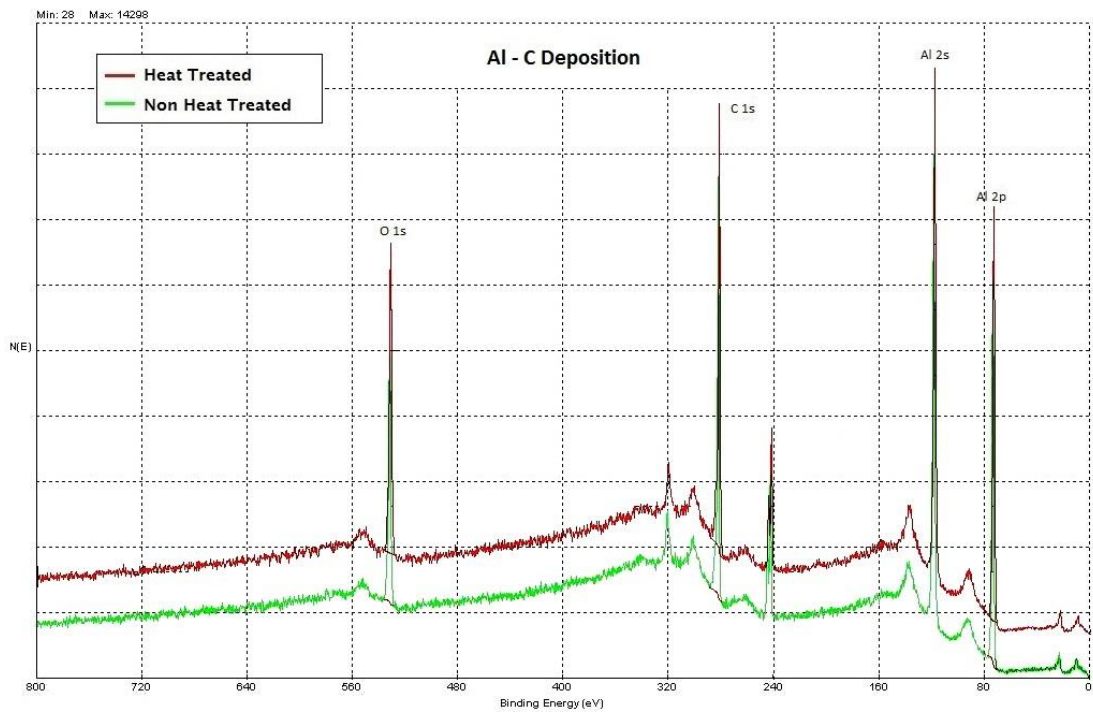


Figure 36. XPS Survey for As Deposited Al – C and Heat Treated Al – C

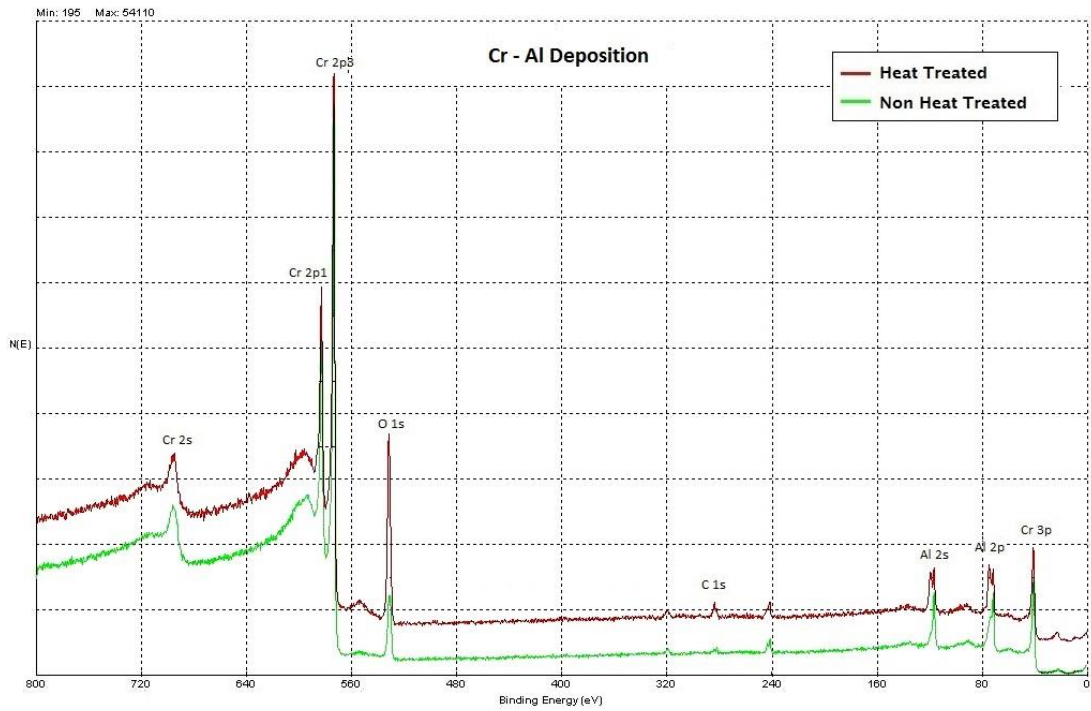


Figure 37. XPS Survey for As Deposited Cr - Al and Heat Treated Cr - Al

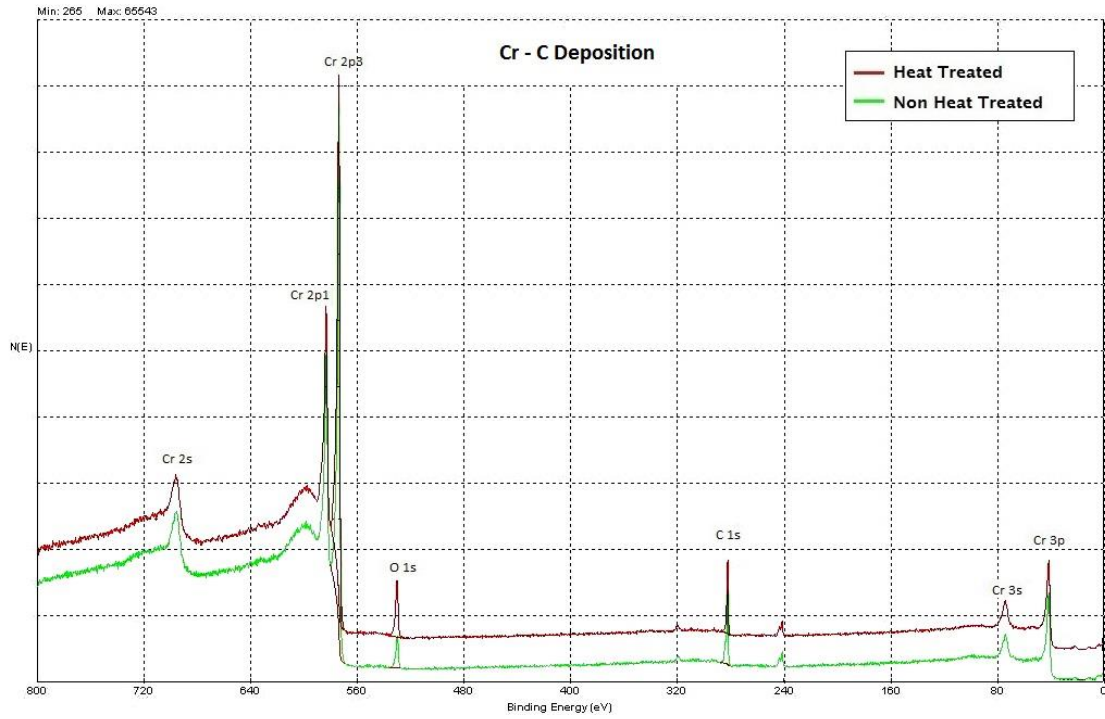


Figure 38. XPS Survey for As Deposited Cr - C and Heat Treated Cr - C

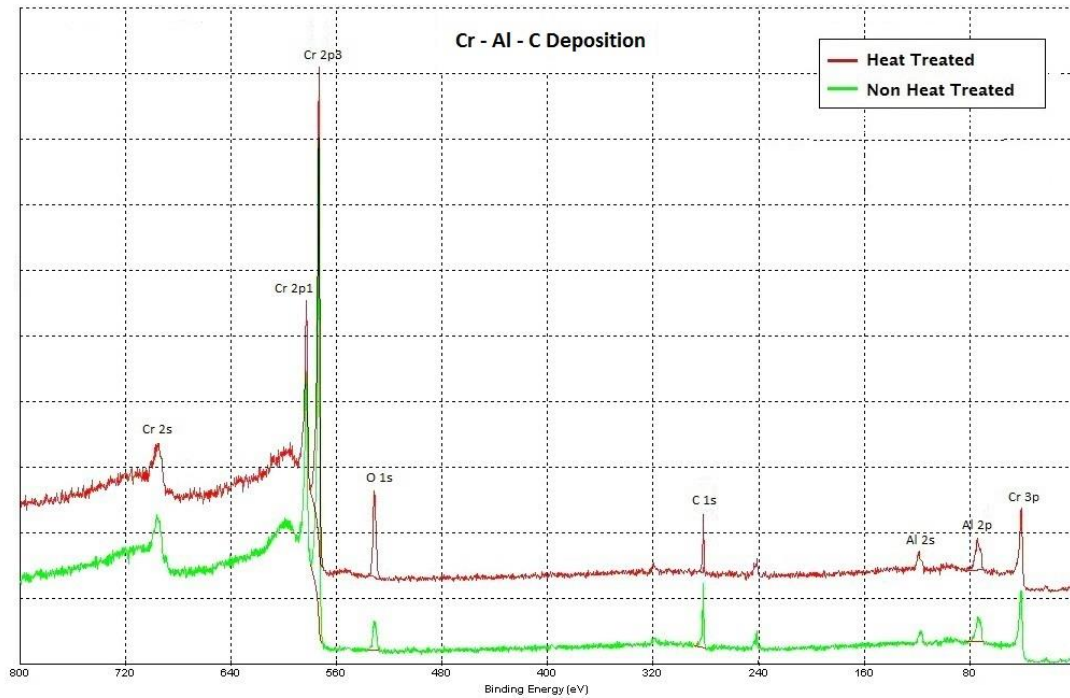


Figure 39. XPS Survey for As Deposited Cr - Al - C and Heat Treated Cr - Al - C

Two important results can be extracted from XPS characterization. First of all, sputter depositions with carbon (Figures 36, 38, and 39) showed the formation of carbides as the carbon peaks (C1s) detected had binding energies of 282 eV, corresponding to a carbide peak in comparison to having a binding energy of 285 eV, which would then indicate graphite or adventitious carbon (Ramqvist, Hamrin, Johnasson, Fahlman, & Nordling, 1968). This corroborates the explanation that samples coated with carbon already had desired phases present before heat treatment. For the case of Cr - C and Al - Cr - C deposition, the phases present were amorphous and therefore this explains why no peaks were detected with the GIXRD before heat treatment.

All sputter deposited coatings except for Cr - Al deposition experienced only minor, negligible changes in their respective binding energies, which could have been

due to the change in their respective binding energies to transition from an amorphous structure to a crystalline structure. Referring to Figures 36, 38, and 39, Cr, Al, C, and O peaks had essentially the same binding energies before and after heat treatment, suggesting that the chemical states of each samples were the same throughout the process. The only significant difference between XPS results for these samples before and after heat treatment is the increase in oxygen concentration detected in heat treated samples, which can be explained by the preferential oxidation of the first couple nanometers of the coating's surface during heat treatment, and also possibly from the slow but natural oxidation of the samples' surfaces after leaving them at room temperature for some time.

Note that the purpose of the XPS is to ensure the formation of carbides after magnetron sputter deposition and to prove that heat treatment did not significantly alter any chemical states of the elements of the deposited films. It also verified that the coatings had desired chemical compositions before heat treatment, the heat treating process was just to result in an amorphous to crystalline structural change within the thin film coatings to allow material characterization using GIXRD.

4.3 Type II Hot Corrosion

4.3.1 Gravimetric Analysis (LTHC)

Coated and uncoated samples were exposed to simulated Type II hot corrosive environment at 700 °C consisting of 2 ppm SO₂ flowing at a rate of 30 cm³min⁻¹ and their mass gain data were collected at time points specified in Section 3.2. The gravimetric analysis results for Type II Hot Corrosion during experimentation are

presented in Figure 40. Uncoated Ni-201 sample experienced the most specific mass gain during exposure testing. All samples with thin film coatings resulted in reduced mass gain when compared to that of uncoated Ni-201 samples.

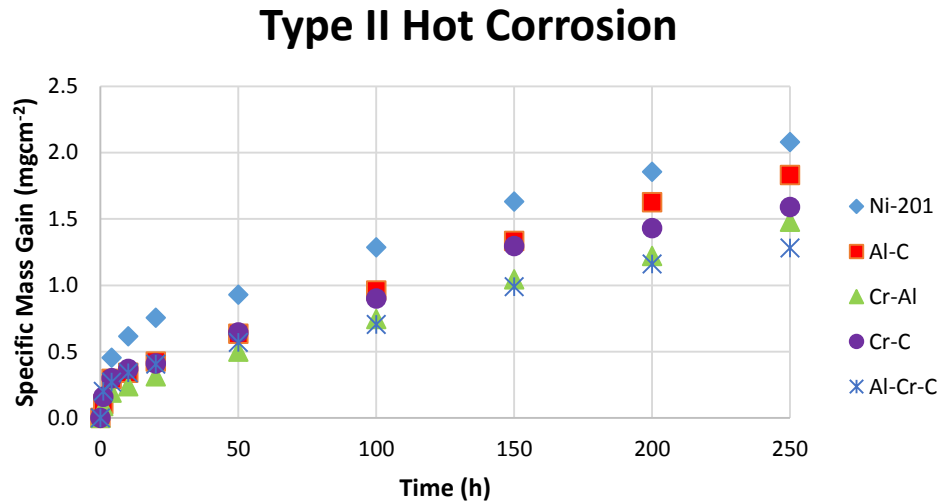


Figure 40. Gravimetric Analysis of Type II Hot Corrosion

There was no observable period of protective scaling for the uncoated Ni-201 sample due to the formation of non-protective scales induced by Na_2SO_4 - NiSO_4 eutectic which accelerated further degradation of the Ni-201 base metal. On the other hand, while Al - C and Cr - C deposited samples did in fact provide some protection against Type II Hot Corrosion within the first 50 hours of exposure, Al - C and Cr - C coated specimens experienced a rapid increase in specific mass gain after that and Cr - Al deposited samples seemed to exhibit similar behavior after 200 hours of exposure. This suggests that the three binary coatings were incapable of providing satisfactory protection against Type II Hot Corrosion for 250 hours. Coating parameters such as increasing coating

thickness and the effects of coating grain sizes could be further examined to improve their protection against this particular hot corrosive mechanism.

The Cr – Al – C coating deposited Ni-201 exhibited the best protection against Type II Hot Corrosion for up to 250 hours, experiencing a specific mass gain of approximately 1.28 mgcm^{-2} , which was the least increase in specific mass in all tested samples. The results of gravimetric analysis for both Cr – Al and Cr – Al – C deposited samples suggest that the XRD and FEM results should indicate formation of continuous chromium oxide and aluminum oxide scales which protects the Ni-201 base metal from severe oxidation due to hot corrosion. In addition to that, results from other materials characterization techniques used should also reinforce the findings from the gravimetric analysis.

4.3.2 XRD Results (LTHC)

Once the samples had their final masses recorded for gravimetric analysis after 250 hours of exposure, they were cleaned with warm deionized water and dried to remove any water soluble compositions that does not provide any protection against corrosion. The samples were then analyzed using GIXRD with the same grazing angle of 6° to determine the phases present on their respective surfaces.

GIXRD results of phases present on the surfaces of the samples (Ni-201, Al - C, Cr - Al, Cr - C, and Cr – Al – C) before and after Type II Hot Corrosion exposure are shown in Figures 41 to 45, respectively.

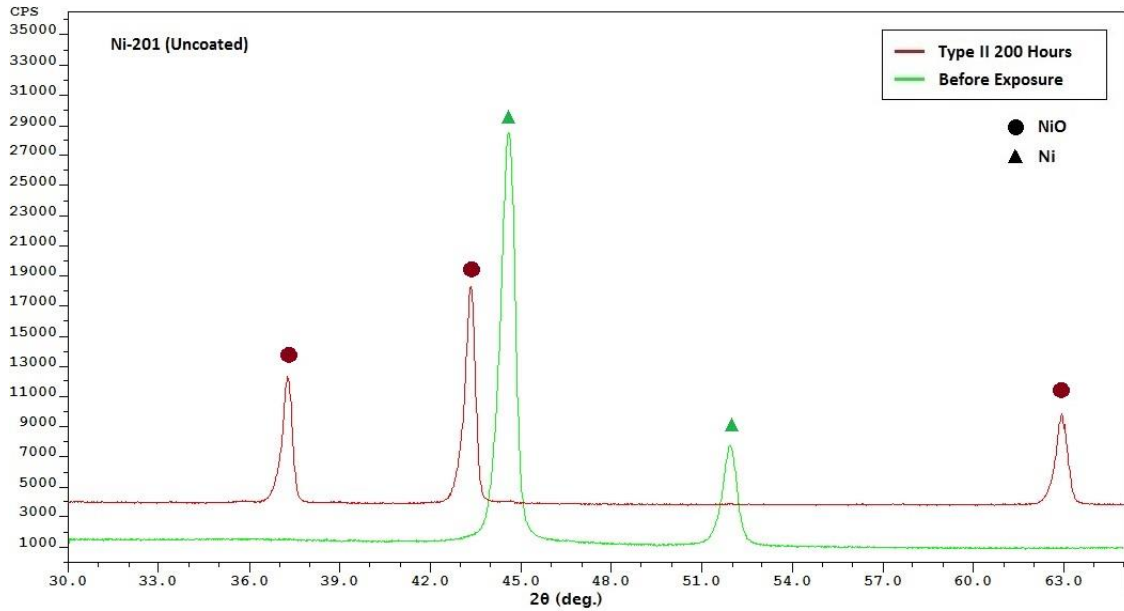


Figure 41. Uncoated Ni-201 after Type II Hot Corrosion Exposure ($t = 250$ h)

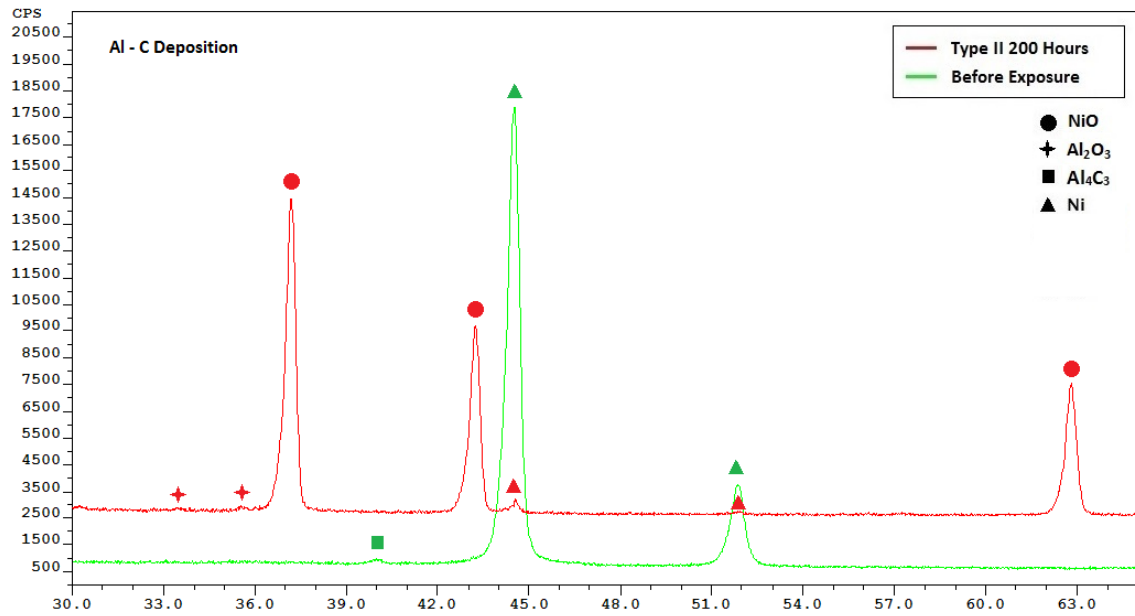


Figure 42. Al - C Coatings after Type II Hot Corrosion Exposure ($t = 250$ h)

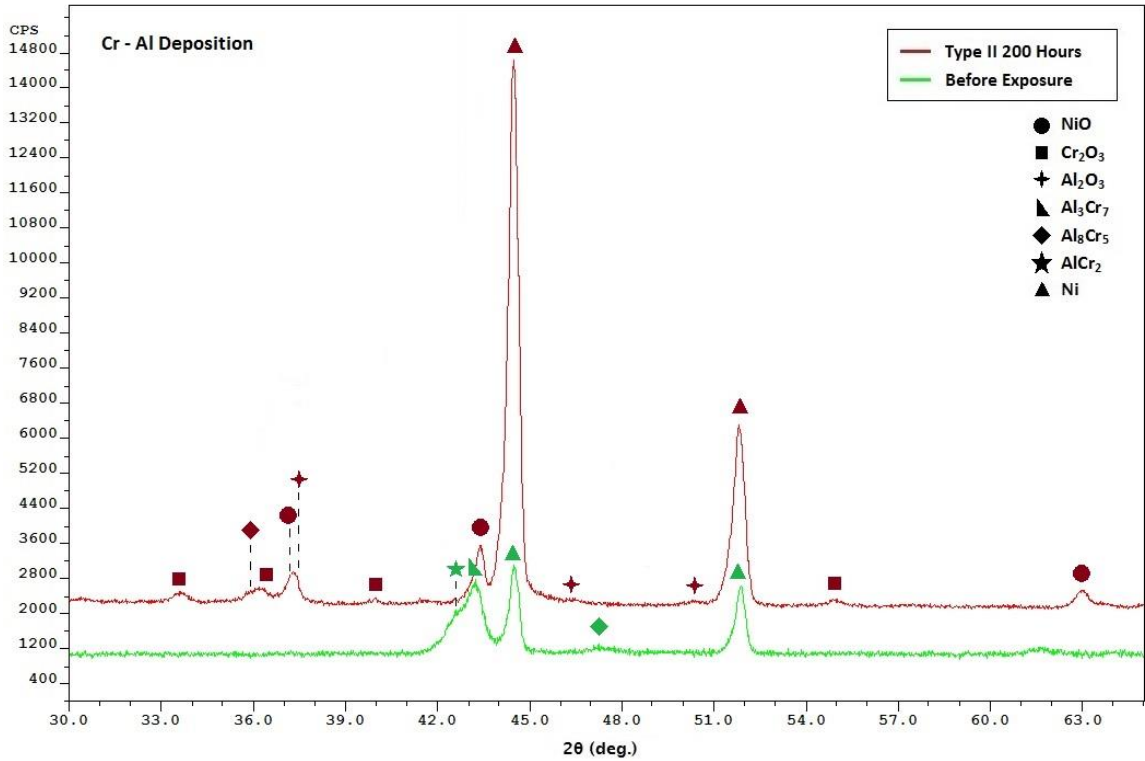


Figure 43. Cr - Al Coatings after Type II Hot Corrosion Exposure (t = 250 h)

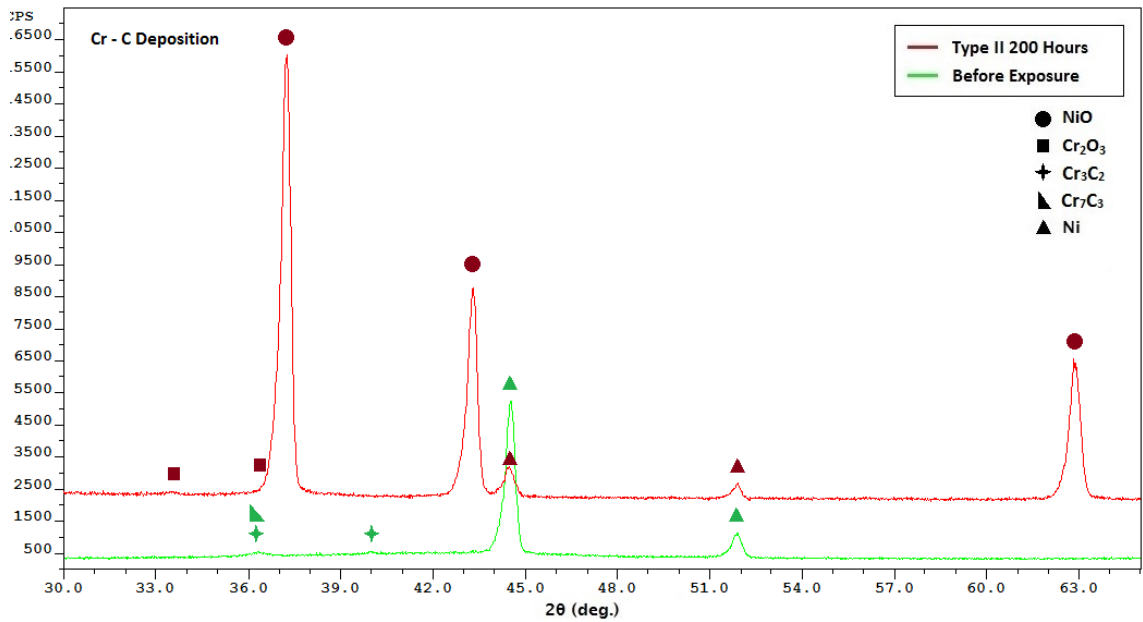


Figure 44. Cr - C Coatings after Type II Hot Corrosion Exposure (t = 250 h)

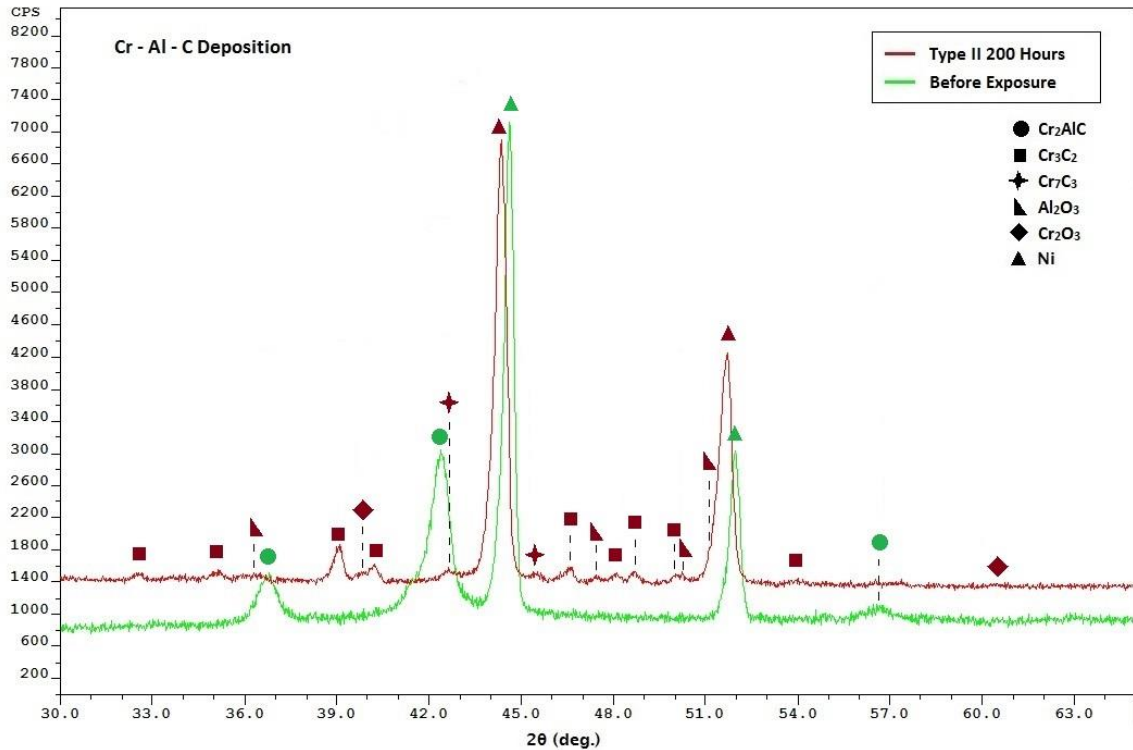


Figure 45. Cr-Al-C Coatings after Type II Hot Corrosion Exposure ($t = 250$ h)

It was determined from GIXRD results that NiO was the main composition found on the surfaces of uncoated Ni-201 samples (Figure 41), Al - C thin film coated samples (Figure 42), and Cr - C thin film coated samples (Figure 44) after 250 hours of exposure in Type II Hot Corrosion.

For both the Al - C and Cr - C coated samples, barely any alumina or chromia scales were found on their respective samples; the peaks indicating the presence of either Al_2O_3 or Cr_2O_3 were so small they were reaching the limitations of the XRD implemented and thus their presence have to be crossed checked with other materials characterization techniques. However, the presence of only NiO on their respective surfaces after 250 hours of exposure suggests that the alumina or chromia scales formed initially have been compromised by the eutectic Na_2SO_4 - NiSO_4 , resulting in the

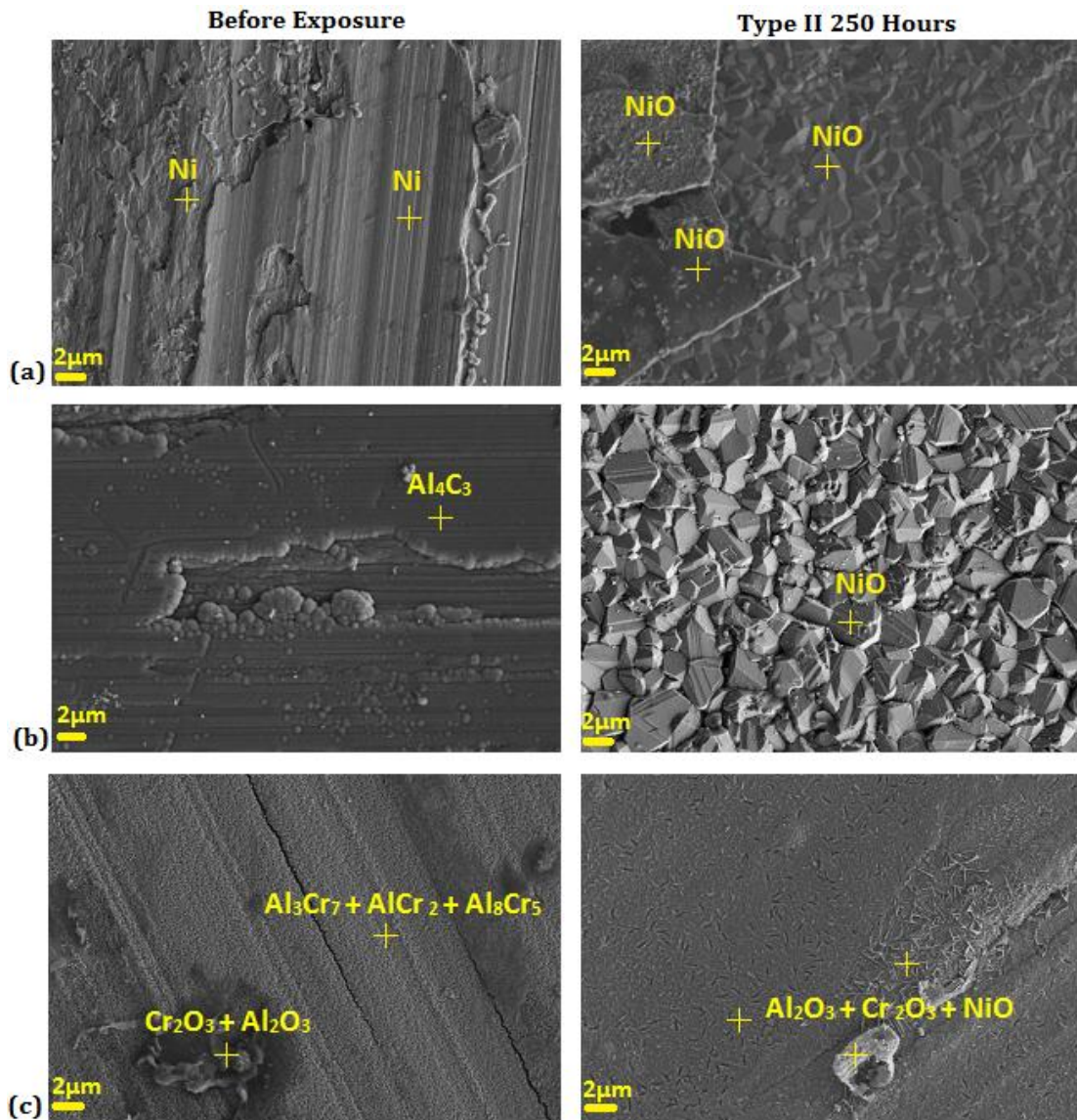
formation of non-protective scales that allowed further oxidation of the base metal (Ni-201 substrate). This would then explain the more rapid mass gain of the Al - C and Cr -C coated samples after 50 hours from gravimetric analysis.

On the other hand, Cr - Al coated samples seemed to be the most protective binary thin film coating; not only both Al_2O_3 and Cr_2O_3 were detected from GIXRD (Figure 43), the results also indicate that the base metal mostly maintained its original composition of Ni, instead of oxidizing into NiO. However, pairing the NiO peaks detected from GIXRD results with the accelerated increase in specific mass as presented in gravimetric analysis results showed that this particular coating was still not as effective as that of Cr - Al - C deposited samples after Type II Hot Corrosion exposure for 250 hours.

Lastly, GIXRD results for Cr - Al - C coated samples (Figure 45) determined the formation of Al_2O_3 and Cr_2O_3 , this particular result when paired with the detection of strong Ni peaks without any indication of NiO on the surface signifies that the coating was able to provide good protection against Type II Hot Corrosion for up to 250 hours. In addition to that, due to the presence of chromium carbide (mainly having the chemical composition Cr_3C_2), it can be hypothesized that this particular coating will still be able to provide further protection against Type II Hot Corrosion by allowing more formation of Cr_2O_3 in a manner similar to that of equation (7) by Li et. al. presented in Section 2.2.3 before experiencing a rapid increase in specific mass and the formation of NiO on the surface.

4.3.3 FEM and EDX (LTHC)

The surface morphologies of all 5 sets of samples before and after Type II Hot Corrosion exposure with their respective chemical compounds determined from EDX is shown in Figure 46.



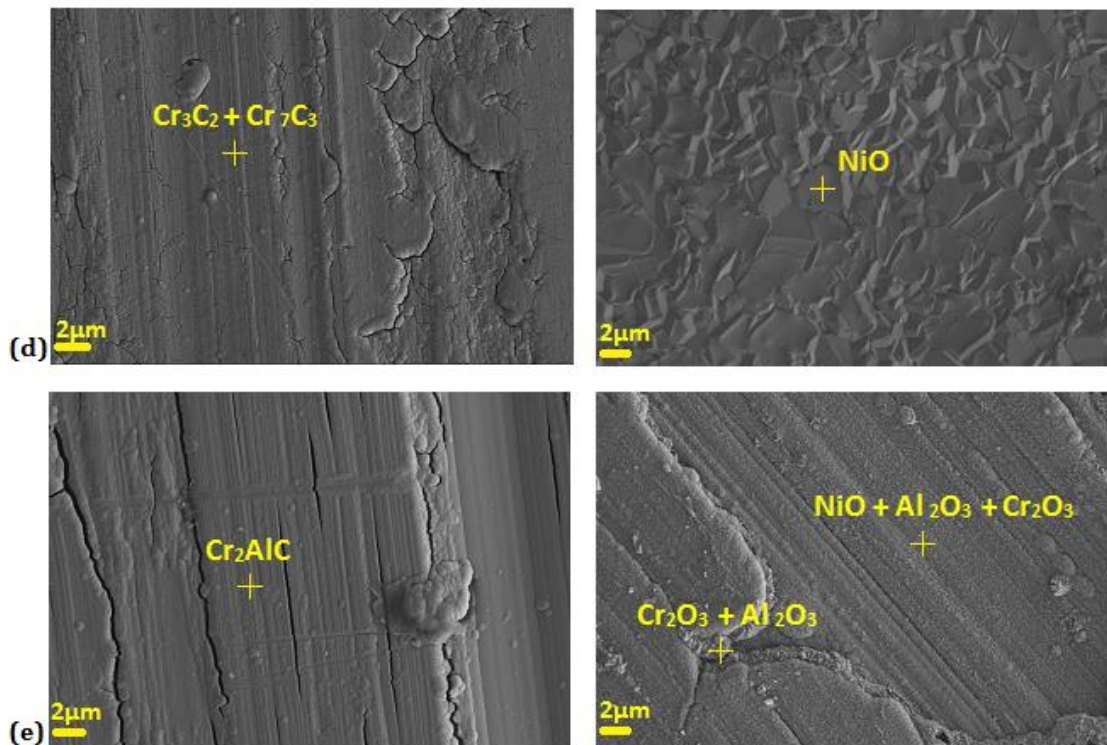


Figure 46. Surface Morphologies before and after Type II Hot Corrosion Exposure of (a) Ni-201, (b) Al - C, (c) Cr - Al, (d) Cr - C, and (e) Cr - Al - C for 250 hours

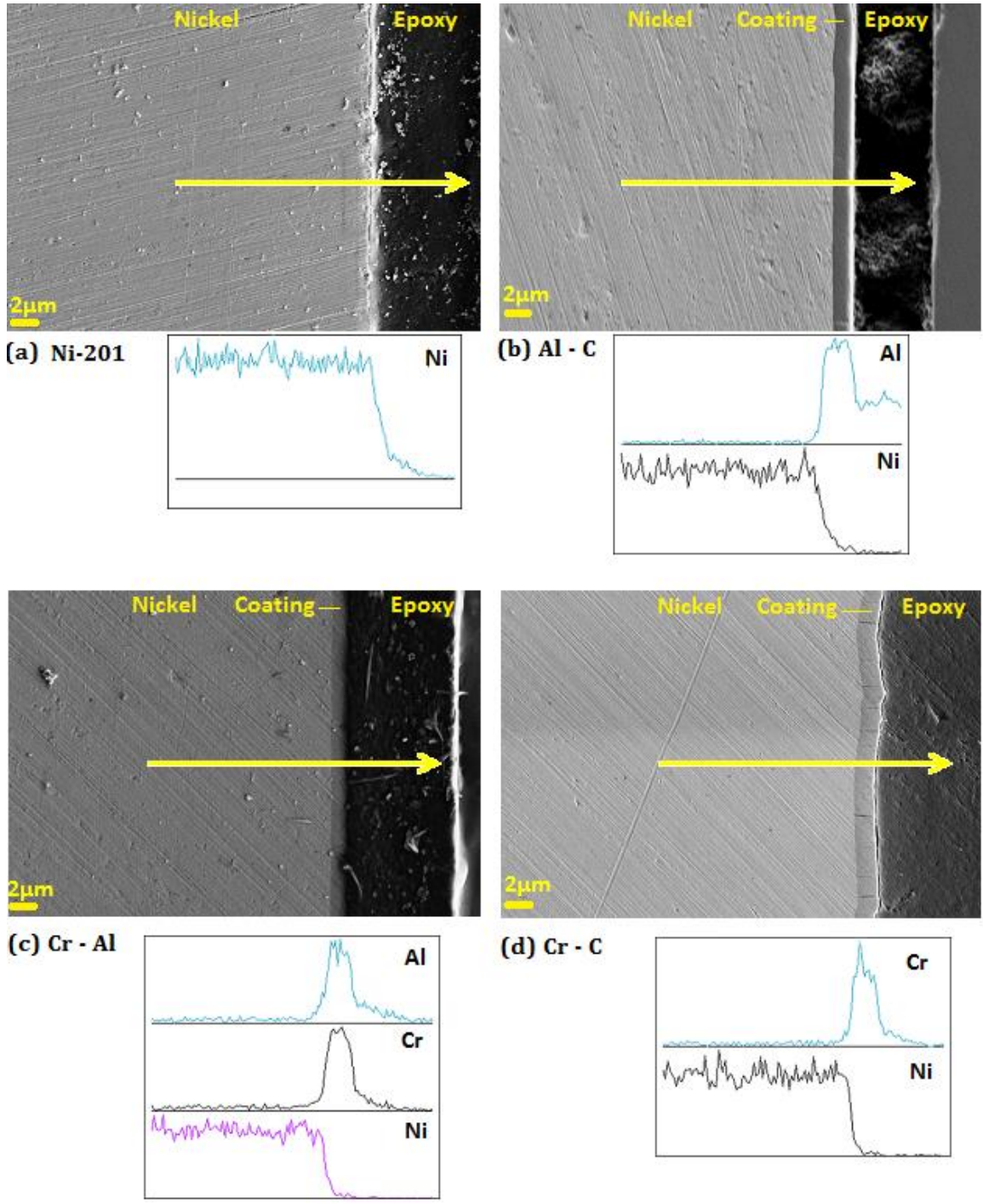
The surfaces of uncoated Ni-201, Al - C coated, and Cr - C coated samples agreed with analysis from GIXRD presented in the previous section as EDX spot scans determined the presence of only NiO on the surfaces of these samples. One important thing to note is that the NiO scales that formed on the uncoated Ni-201 were not continuous and showed localized spallation throughout the surface of the sample; whereas NiO scales formed on the surfaces of Al - C coated and Cr - C coated samples were continuous and both had similar grain sizes and crystalline structures. This suggests that the NiO present on uncoated Ni samples are not protective when compared to that of NiO formed on Al - C and Cr - C coated samples.

While Al_2O_3 and Cr_2O_3 have been known to provide protection against hot corrosion, the change in composition of Na_2SO_4 to result in more acidic or more basic salt eutectic due to environmental conditions as described in Section 2.1.2 contributes to oxygen ions (O^{2-}) within the melt. This satisfies the requirements for the protective alumina and chromia coatings to dissolve according to reactions (1) and (2), resulting any initially protective Al_2O_3 or Cr_2O_3 in Al – C and Cr – C coated samples to completely dissolve during Type II Hot Corrosion exposure.

On the other hand, EDX spot scans of Al - Cr and Cr - Al - C coated samples after Type II exposure for 250 hours showed the formation of crystalline Al_2O_3 and Cr_2O_3 with some NiO on their surfaces. The presence of NiO on the surfaces was suggested to be due to the diffusion of Ni from the base metal across the coating materials and then oxidizing on the surface. It was hypothesized that NiO present on the Cr - Al coated samples were thicker than that of MAX phase coated samples, resulting NiO peaks to be detected from GIXRD for Cr – Al coated samples but not in Cr – Al – C coated samples.

Cr - Al - C coated samples showed a continuous, protective layer of chromia and alumina scales throughout the samples; whereas the Cr – Al coated samples had crevices of approximately $0.7 \mu\text{m}$ on its surface which had comparatively higher concentration of NiO (although Al_2O_3 and Cr_2O_3 were still present). This shows the regions in which oxidation of the base metal would preferentially occur if this particular sample was exposed to Type II Hot Corrosion for a longer period of time, which could be one reason contributing to the less protection against Type II Hot Corrosion of Cr - Al samples when compared to that of Cr - Al - C samples.

The cross sections of samples before and after Type II Hot Corrosion exposure were also examined with EDX line scans and are presented in Figure 47.



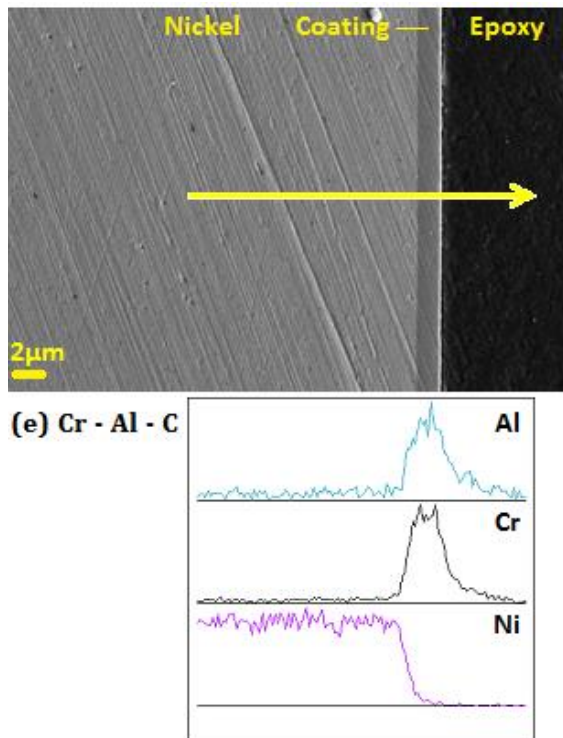
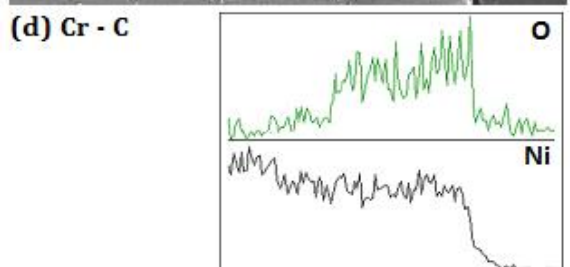
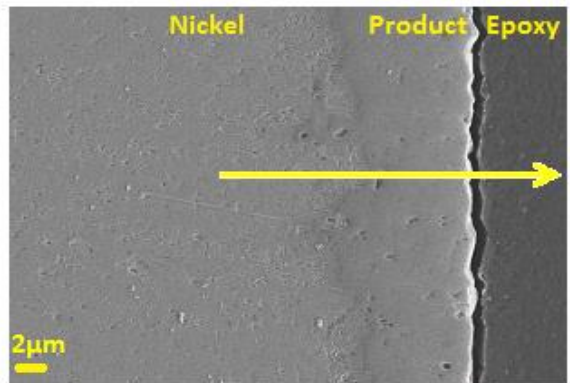
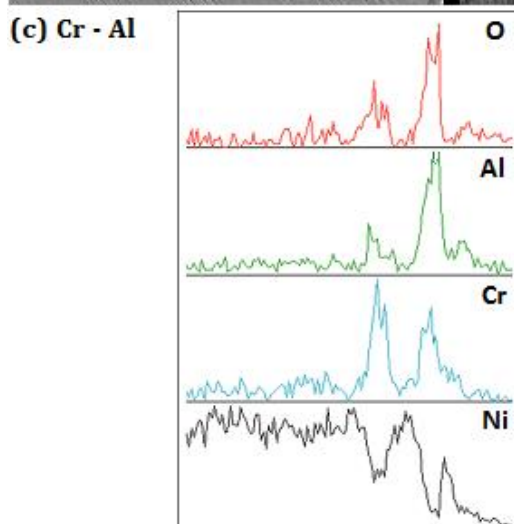
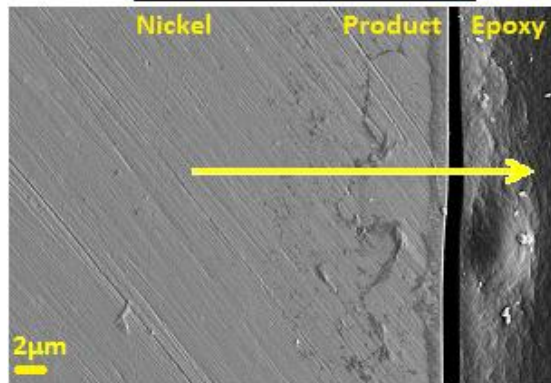
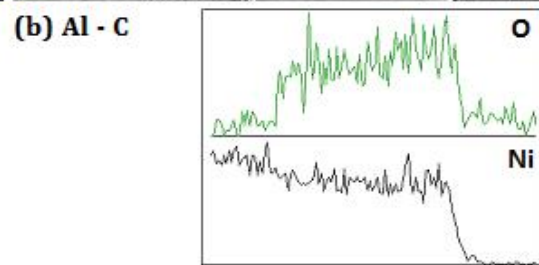
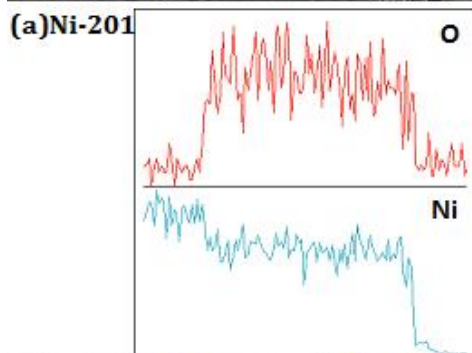
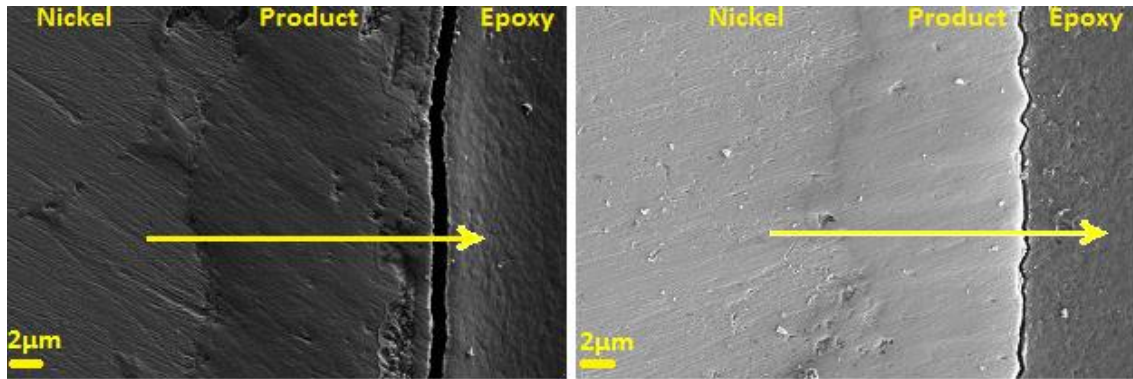


Figure 47. Cross Sections with EDX Line Scans of (a) Ni-201, (b) Al - C, (c) Cr - Al, (d) Cr - C, and (e) Cr - Al - C Samples before Exposure

Note that although carbon (C) was an element of interest throughout the study, it was not included in the line scans as C detected by the FESEM implemented were mainly noise due to the use of a carbon based epoxy resin and does not add any value to the EDX analysis of the samples. Apart from that, the coating thicknesses of each sample in Figure 47 were cross checked with the results obtained from profilometry (Table 8) and it was verified that both methods presented very similar results. The cross sections of each sample with their corresponding EDX line scan results after 250 hours of testing is presented in Figure 48.



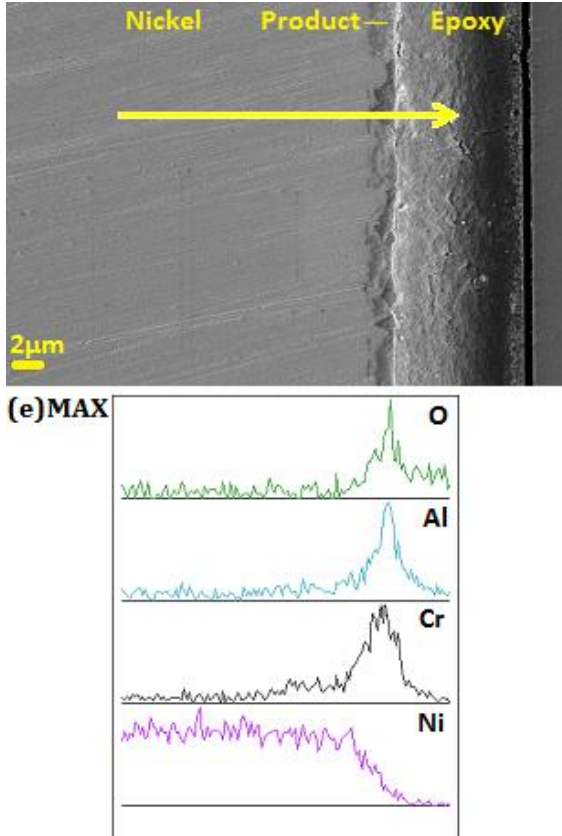


Figure 48. Cross Sections with EDX Line Scans of (a) Ni-201, (b) Al - C, (c) Cr - Al, (d) Cr - C, and (e) Cr - Al - C Samples after Type II Hot Corrosion Exposure for 250h

EDX line scan results showed that Ni and O, in the form of NiO, were the main elements present in Ni-201, Al - C coated samples, and Cr - C coated samples. This once again agrees with the findings from both GIXRD and surface spot scans. Carrying out EDX line scans also allowed the determination of the depth of oxide scales that formed during the 250 hours of exposure. It was measured that uncoated Ni-201 had an average oxide scale of 16 μm ; whereas that of Al - C and Cr - C coated samples were 14 μm and 10 μm , respectively, signifying that uncoated Ni-201 samples experienced the most severe oxidation followed by Al - C coated samples and then Cr - C coated samples.

The EDX line scan of Cr - Al coated samples after Type II Hot Corrosion exposure testing was more complicated than the earlier cases; while an average of 10 μm of oxide scales was detected in the samples, the intensity of O peaks detected were not as high as that of the uncoated Ni-201 samples and the other two binary thin film coated materials. Referring to Figure 48c, the first 0.75 μm of the sample consisted of a combination of Ni and NiO with some Al_2O_3 and Cr_2O_3 , at regions approximately 3 μm to 7 μm into the sample high concentration of Al_2O_3 and some Cr_2O_3 were detected and a scattered region of high Cr_2O_3 concentration was observed at regions 7 μm to 10 μm into the sample. The interdiffusion between Ni, Al, and Cr were postulated to be the mechanism behind the findings for this particular case but should be further examined to verify the results.

Lastly, it was determined that the MAX phase coated samples (Figure 48e) provided the best protection against Type II Hot Corrosion; not only the oxide scales grown had only an average length of 2 μm , a high concentration of Al and Cr were detected within this region, indicating the formation of continuous, protective layer of Al_2O_3 and Cr_2O_3 after Type II Hot Corrosion exposure for 250 hours.

4.4 Type I Hot Corrosion

4.4.1 Gravimetric Analysis (HTHC)

The initial procedure for carrying out Type I Hot Corrosion exposure testing was to be identical to that of Type II Hot Corrosion exposure; however, it was also predicted to have higher rates of oxidation and the time between gravimetric analysis and the total time of exposure was altered slightly from Type II Hot Corrosion exposure testing and

the final procedure implemented has been documented in Section 3.2. Gravimetric analysis for samples after 50 hours of exposure under Type I Hot Corrosion is presented in Figure 49.

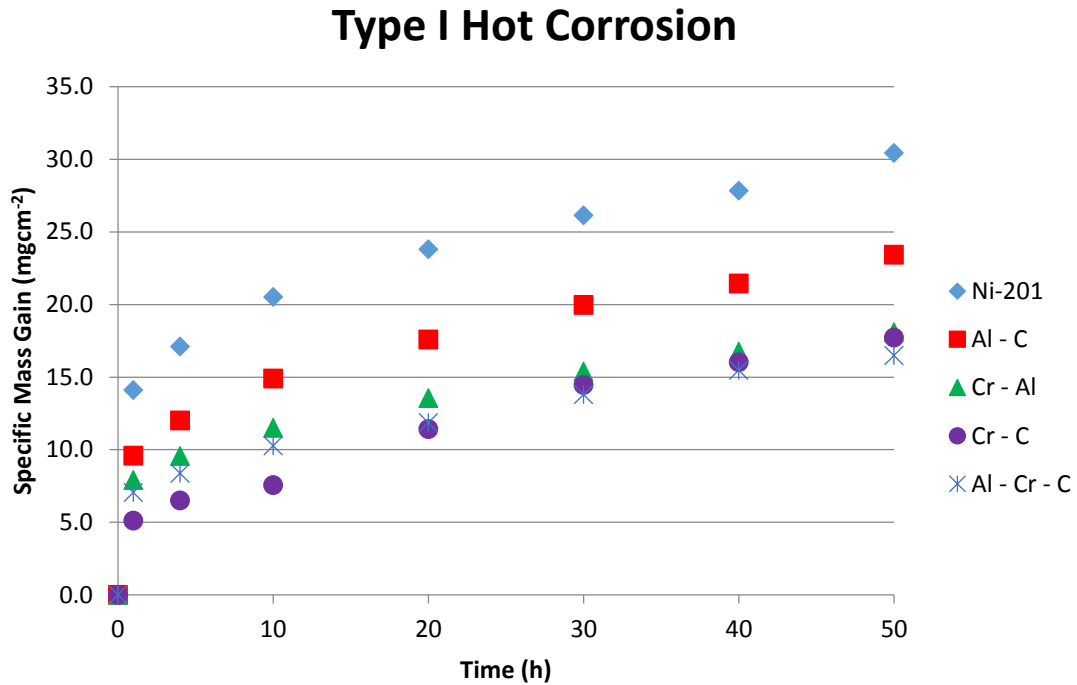


Figure 49. Gravimetric Analysis of Type I Hot Corrosion

The experiment was stopped after 50 hours of Type I Hot Corrosion exposure as the specific mass gain experienced by all the tested samples were several orders of magnitude larger than that experienced by the same samples during Type II Hot Corrosion exposure testing. It was also determined that all coatings had effectively lost their abilities to provide further protection against Type I Hot Corrosion and further exposure would not have provided additional useful information for the purpose of the study.

Gravimetric analysis results of Type I Hot Corrosion exposed samples were also compared to that of other publications. A 10 μm Cr_2AlC coating exposed to ambient air at 900 °C for 20 hours was reported to experience a specific mass gain of 6 mgcm^{-2} (Li, Li, Xiang, Lu, & Zhou, 2011); whereas in another study, Cr_2AlC coatings that were 15 μm thick indicated a specific mass increase of 7.8 mgcm^{-2} after being exposed to Type I Hot Corrosion for 20 hours (Lin, Li, Wang, & Zhou, 2007). These results when compared to the specific mass gain of 11.85 mgcm^{-2} after 20 hours of Type I Hot Corrosion exposure for the 1.8 μm Cr_2AlC thin film coating deposited seemed to yield coherent results, as one would expect thickness to affect the protective capabilities of the same coating, where thicker coatings should be able to result in a thicker layer of oxide layer formation to act as an oxygen barrier, preventing further oxidation of the material from occurring.

The determination that all coatings had lost their protective capabilities against Type I Hot Corrosion was not only based on results from gravimetric analysis, but also from direct observation of exposed samples after 50 hours of exposure to Type I Hot Corrosive environments. The physical appearances of all exposed samples after 250 hours of Type II Hot Corrosion and that after 50 hours of Type I Hot Corrosion is shown in Figure 50.

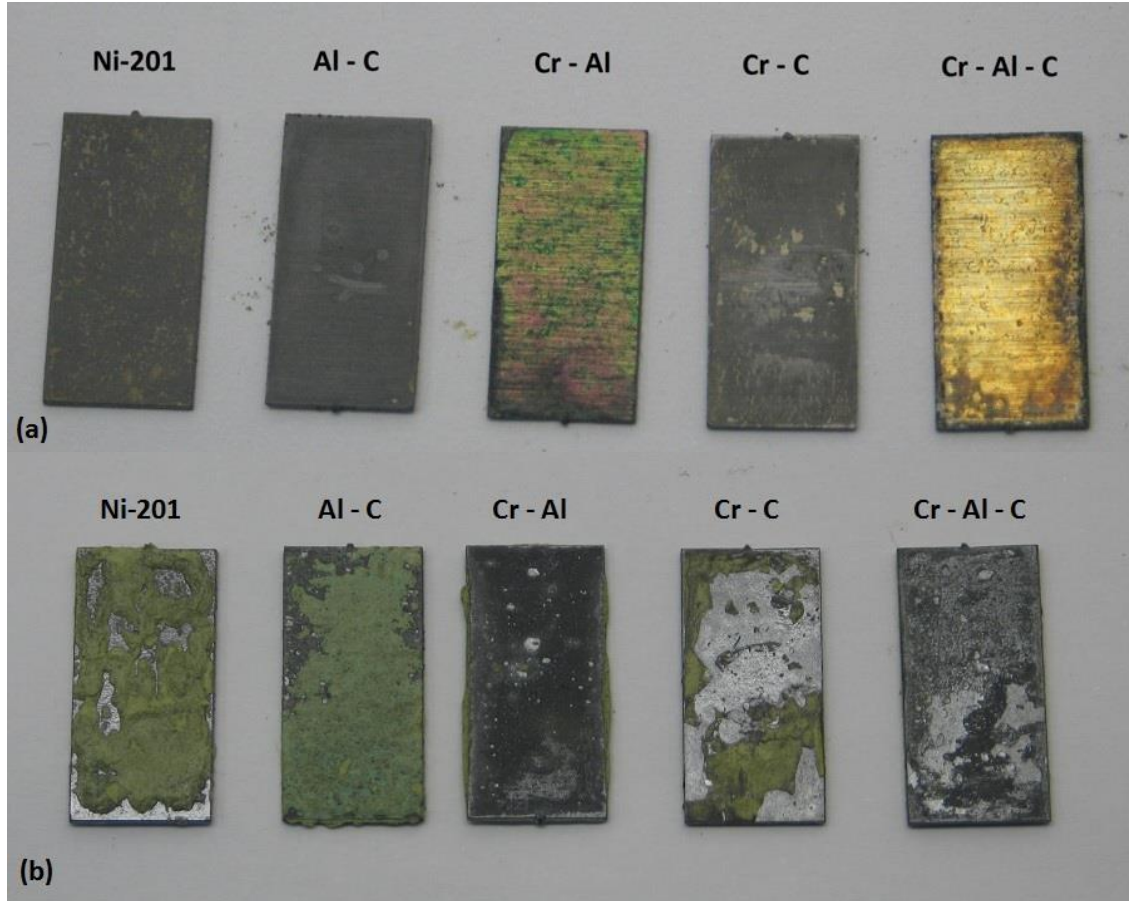


Figure 50. (a) Samples after Type II Hot Corrosion Exposure for 250 hours, (b) Sample after Type I Hot Corrosion Exposure for 50 hours

As presented in the Section 4.3, MAX phase thin film coatings were the most effective thin film coating against Type II Hot Corrosion. Referring to Figure 50(a), even after exposure to Type II Hot Corrosion for 250 hours, MAX phase coated samples still showed a golden tint similar to that of the heat treated sample before exposure testing (Figure 31). However, from direct observation of the MAX phase coated samples in Figure 50(b), it was deduced that the thin film coating had been compromised and have completely reacted with molten Na_2SO_4 after Type I Hot Corrosion testing.

All the other samples exposed to Type I Hot Corrosion for 50 hours showed the same significant increase in severity of oxidation when comparing them to samples after Type II Hot Corrosion exposure for 250 hours. Cr – Al coated samples looked similar to the MAX phase coated samples after Type I Hot Corrosion exposure. On the other hand, uncoated Ni-201, Al – C coated, and Cr – C coated samples had formation of greenish scales on their surfaces which have been reported by Eliaz et. al. as a macroscopic feature of Type I Hot Corrosion. (Eliaz, Shemesh, & Latanision, 2002). This reinforces the idea that all thin film coatings deposited for experimentation did not provide sufficient protection against Type I Hot Corrosion.

4.4.2 XRD Results (HTHC)

Samples exposed to Type I Hot Corrosion for 50 hours had their surface compositions analyzed using GIXRD and their results presented in Figure 51. As predicted from gravimetric analysis, all coatings had already lost their protective capabilities after 50 hours of exposure testing, resulting the base metal to further oxidize and all tested samples showed only the presence of NiO.

Any initially protective Al_2O_3 and Cr_2O_3 that formed during exposure for thin film coated samples were compromised by molten Na_2SO_4 , resulting the dissociation of the protective scales according to reaction (1) and reaction (2) (Birks, Meier, & Pettit, 2006), which then exposes the base metal and allowed the nickel substrate to oxidize into NiO.

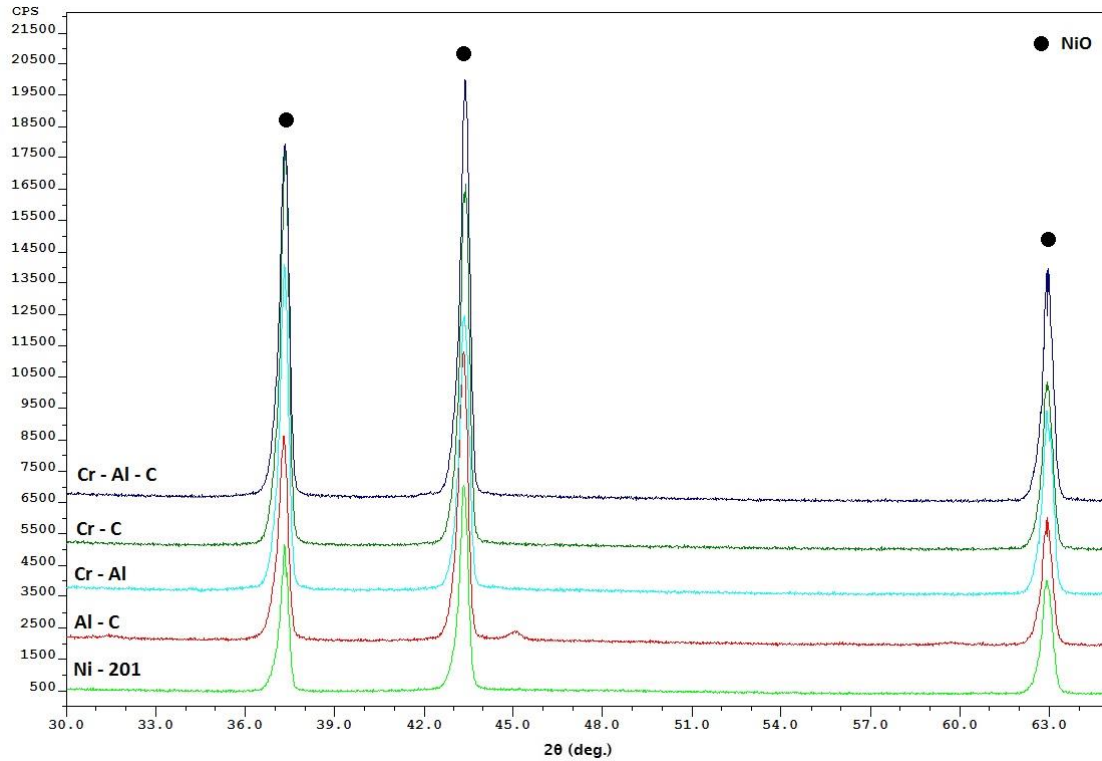


Figure 51. GIXRD Results of Samples after Type I Hot Corrosion Exposure ($t = 50$ h)

4.4.3 FEM and EDX (HTHC)

The surface analysis provided by GIXRD in the last section was also cross checked using the FEM along with its EDX spot scan and line scan capabilities and the surfaces of all samples, along with spot scans of features of interest after Type I Hot Corrosion exposure for 50 hours are presented in Figure 52.

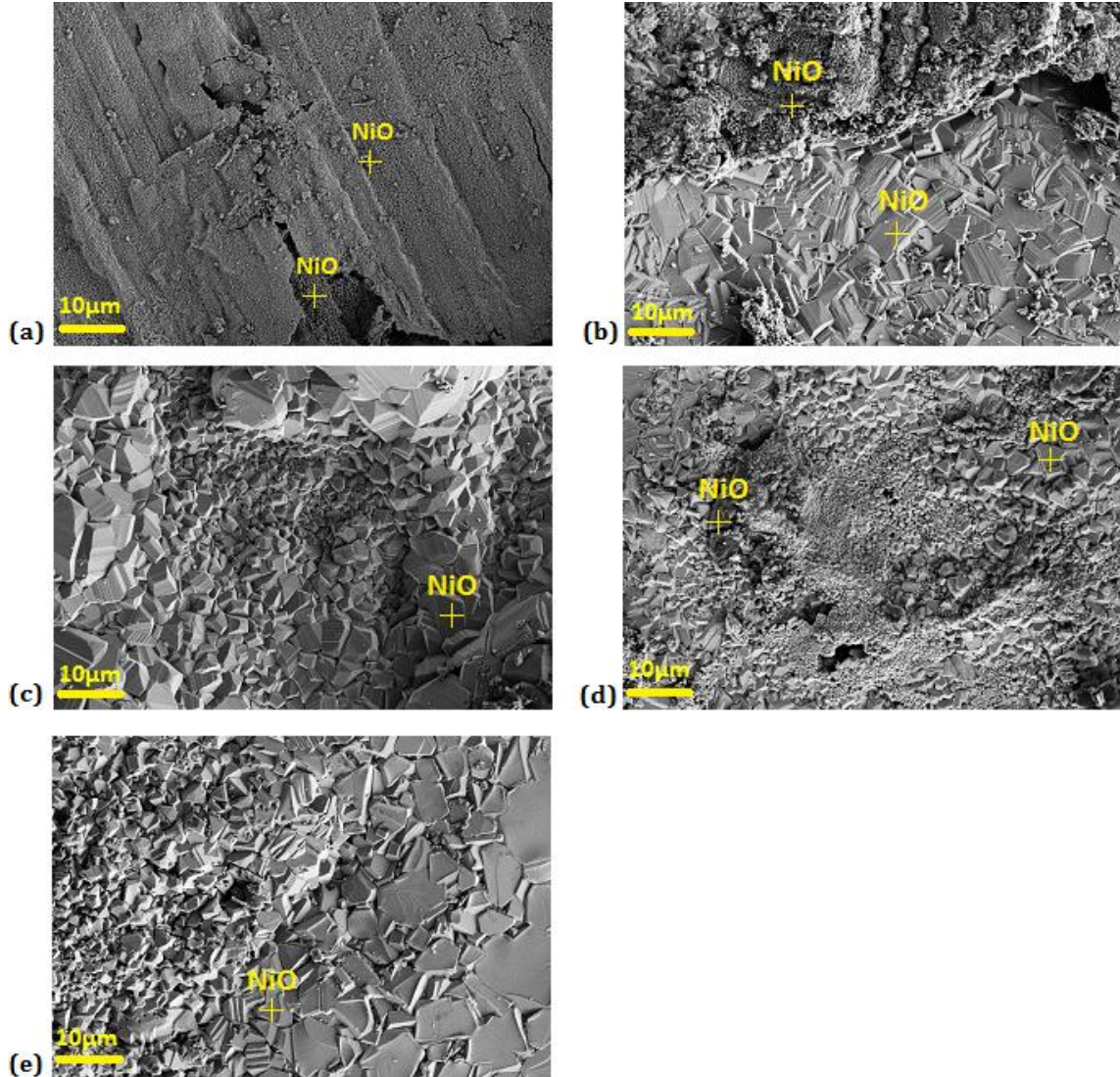


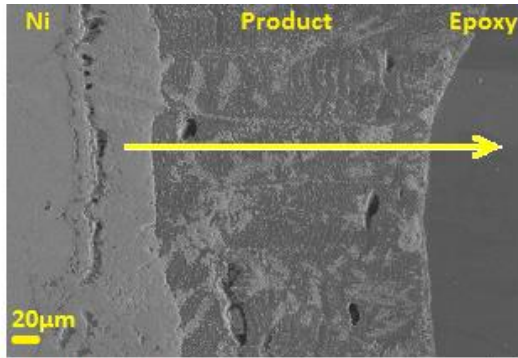
Figure 52. Surface Morphologies after Type I Hot Corrosion Exposure Testing of (a) Ni-201, (b) Al - C, (c) Cr - Al, (d) Cr - C, (e) Cr - Al – C Samples for 50 hours

All samples exposed to Type I Hot Corrosion showed only the presence of NiO on their respective surfaces. Referring to Figure 52(a) and Figure 52(b), NiO that formed on Ni-201 and Al – C coated samples not only had smaller grain sizes when compared to that of the other samples, the presence of cracks on their surfaces indicate that the NiO scales are susceptible to localized spallation which then exposes the base metal for further oxidation.

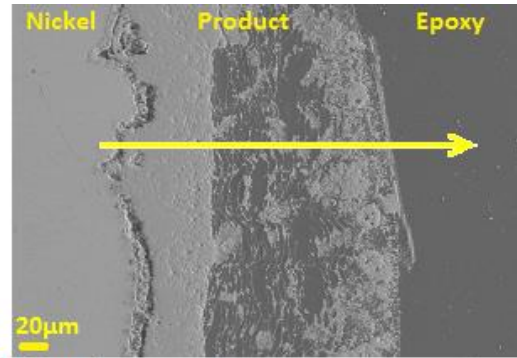
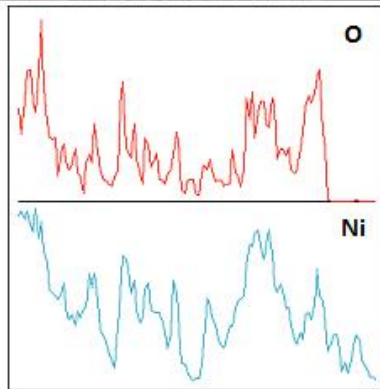
On the other hand, for Cr – Al coated samples and MAX phase coated samples, NiO scales that formed exhibited surface morphologies similar to that of Al – C and Cr – C coated samples after Type II Hot Corrosion exposure testing, Figure 42(b) and Figure 42(d), where the thin film coatings have been completely dissociated but NiO scales that formed on the surfaces were still relatively continuous.

However, NiO scales of smaller grain sizes were also detected in both Figure 52(c) and Figure 52(e), indicating that the initially continuous NiO scales might have experienced a deterioration in grain size due to hot corrosion, in which continuous exposure to the same corrosive environment will eventually result in the formation of NiO that are susceptible to cracks and localized spallation. This grain size transition is evident in Cr – C coated samples, Figure 52(d), where its surface not only had continuous NiO with grain sizes comparable to both Cr – Al and MAX phase coated samples after Type I Hot Corrosion testing, but also localized spallation that does not provide any oxidation protection to the base metal.

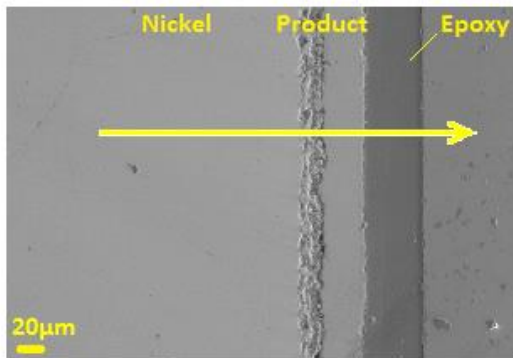
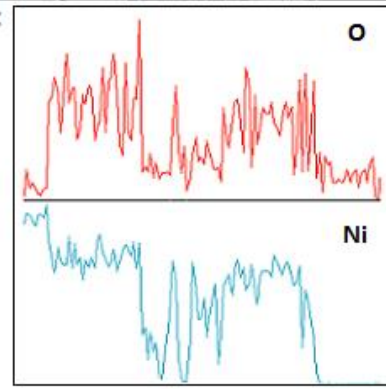
In addition to carrying out surface analysis using the FEM, EDX line scans of the samples after Type I Hot Corrosion exposure testing were also performed and their results presented in Figure 53.



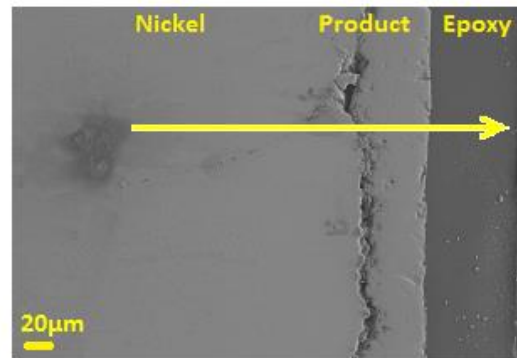
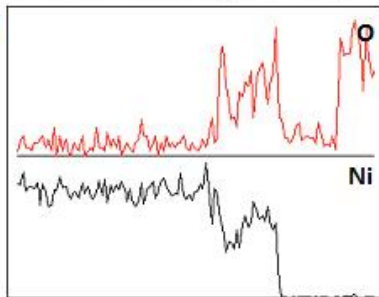
(a) Ni-201



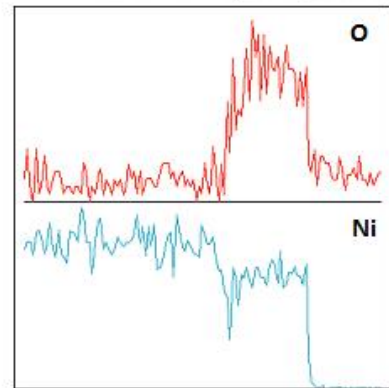
(b) Al - C



(c) Cr - Al



(d) Cr - C



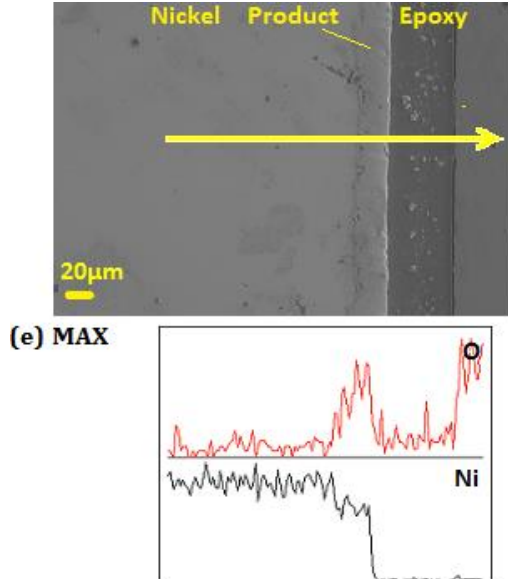


Figure 53. Cross Sections with EDX Line Scans of (a) Ni-201, (b) Al - C, (c) Cr - Al, (d) Cr - C, and (e) Cr - Al - C Samples after Type I Hot Corrosion Exposure for 50 Hours

The oxide layer that forms for uncoated Ni and Al – C coated samples were a lot thicker than that of the other tested samples. Referring to Figure 53(a) and Figure 53(b), both samples suffered from severe oxidation and NiO scales formed were porous and does not seem to provide protection to the base metal. The average oxide scale growth for uncoated Ni and Al – C coated samples were detected to be more than 60 μm and were significantly more porous than that formed on all other samples.

From Figure 53(c) and Figure 53(d), Cr – C and Cr – Al coated samples showed oxide scale growth lower than that of uncoated Ni samples and Al – C coated samples, approximately 42 μm and 35 μm , respectively; however, the oxide boundary layer between Ni and NiO showed cracks which indicate local spallation of NiO. It would be a valid prediction that both samples will slowly trend towards having oxide scale formation similar to that of Figure 53(a) and Figure 53(b) if they were exposed to Type I Hot Corrosion for a longer period of time.

Lastly, while the MAX phase coated samples showed only NiO formation, indicating the complete dissociation of Al_2O_3 and Cr_2O_3 scale during exposure, the Ni, NiO boundary was still continuous and the NiO scale had an average thickness of 28 μm . This shows that although MAX phase coating did not hold up after Type I Hot Corrosion exposure, it was still the most effective protective coating when compared to all other protective thin film coatings experimented with during exposure testing.

In addition to that, the continuous, uniform oxide scale that forms on the surface of the samples show the importance of having similar coefficient of thermal expansion between thin film coating materials and their base alloys, as MAX phase coatings had the most similar coefficient of thermal expansion to Ni-201 compared to that of all other coating materials used. The thickness of the coating materials could be increased and exposure testing carried out once again to investigate if coating thickness greatly influences the Type I Hot Corrosion behavior of the thin film coatings used for experimentation.

CHAPTER FIVE

CONCLUSION

Binary and ternary thin film coatings with chromium, aluminum, and carbon as base elements were developed and deposited onto Ni-201 alloy using the Angstrom magnetron sputtering system in Montana State University, Bozeman. The working recipe for sputter deposition was developed by determining the deposition rates of carbon, chromium, and aluminum and manipulating their respective power sources to yield desired coating stoichiometry (Al_4C_3 , AlCr_2 , Cr_3C_2 , and Cr_2AlC). The samples were heat treated at 500 °C for 1 hour in a low pressure furnace (6×10^{-2} mTorr) directly after magnetron sputtering deposition.

All magnetron sputtering deposited coatings were measured to have thicknesses of approximately 1.5 μm with all coating material having good adhesion to the base metal when examining them with Scanning Electron Microscopy (SEM); the samples were also characterized using Grazing Incident X-Ray Diffraction (GIXRD) and X-Ray Photoelectron Spectroscopy (XPS) to determine the phases present after heat treatment. For the binary elemental deposition, Al – C deposition resulted in formation of Al_4C_3 , Cr – Al deposition yielded three phases, AlCr_2 , Al_3Cr_7 and Al_8Cr_5 , and the Cr – C deposition produced two chromium carbide phases, Cr_3C_2 and Cr_7C_3 . For the Cr – Al – C ternary deposition, Cr_2AlC coatings were successfully deposited onto Ni-201.

The thin film coated samples were then exposed to simulated Type II Hot Corrosion for 250 hours and Type I Hot Corrosion for 50 hours and the protective

capabilities of each binary and ternary thin film coating material under hot corrosion were analyzed using gravimetric analysis, FEM, GIXRD, and EDX.

It was determined that Al – C and Cr – C coated samples had their coating materials completely dissolved after Type II Hot Corrosion exposure for 250 hours; Al_2O_3 and Cr_2O_3 that formed on Al – C and Cr – C coated samples in the beginning started dissociating due to Type II Hot Corrosion, exposing the base metal and in the end did not provide protection against the formation of NiO. However, the samples showed a reduction in mass gain when compared to gravimetric results of uncoated Ni-201 samples, showing that both thin film binary coating did provide protection against Type II Hot Corrosion before dissolving into the Na_2SO_4 - NiSO_4 eutectic.

The last binary coating (Cr – Al) and the ternary Cr – Al – C thin film coatings showed good oxidation resistance against Type II Hot Corrosion for up to 250 hours. Continuous Al_2O_3 and Cr_2O_3 scales were detected from EDX line scans of both samples after exposure testing and a thicker oxide scale was found for the Cr – Al samples when compared to that of Cr – Al – C samples, indicating that the ternary Cr_2AlC thin film coating provided better resistance against Type II Hot Corrosion when compared to that of the Al_3Cr_7 and Al_8Cr_5 phases present in the Cr – Al deposition.

However, results from Type I Hot Corrosion testing indicate that 1.5 μm binary and ternary chromium, aluminum, and carbon coatings were not sufficient in providing long term protection against Type I Hot Corrosion. All thin film coating materials had completely dissociated, resulting in the formation of only NiO scales on the samples. Improving the hot corrosion resistance of the thin film coatings, especially against Type I

Hot Corrosion will therefore be the main focus for future work in the hot corrosion research group following this thesis.

Since all thin film coatings were not sufficient for satisfactory protection against Type I Hot Corrosion, it is recommended that the coating thicknesses be increased to approximately 5 μm . This should not only allow the binary Al – C and Cr – C coatings to exhibit improved Type II Hot Corrosion resistance, but also improve the overall Type I Hot Corrosion resistance to all coating materials as thicker coating material should not only provide the means for more protective Al_2O_3 and Cr_2O_3 scales to form, but the thicker coating material should also be able to mitigate the diffusion of Ni through coating materials, which was one mechanism determined from experimentation that can result in the failure of the thin film coatings.

The deposition rate of carbon targets for magnetron sputtering should also be improved and the working recipe modified to efficiently sputter deposit thin film coatings thicker than that used in this thesis. This could be done by using the RF power source for carbon sputtering and determining if the maximum allowable power supplied to the carbon target will result in deposition rates higher than that of the current limiting deposition rate of 80 nmh^{-1} .

Although RF sputtering would generally result in lower deposition rates than that of DC sputtering, it prevents the sputtering target from overheating, allowing the sputtering of carbon targets at higher power that could result in a higher achievable deposition rate. The sputter deposition process can also be improved and sped up with the use of sputtering targets that already contains desired stoichiometry so future hot

corrosion work with thin film Cr, Al, C coatings can focus more on the performance of the coating materials, not the thin film deposition process.

In the future, the effects of the grain size of thin film coatings could also be examined to determine if the protective capabilities of thin film materials can be further improved by manipulating their mechanical properties. Properties such as the density of protective coatings on substrate alloys has been reported to directly affect their erosion resistance (Zheng & Bu, 1990; Davis, Boone, & Levy, 1986), and can be used as a tool to further improve hot corrosion resistance of each coating material. The effects of time and temperature of heat treatment to the thin film coatings should also be studied to determine the optimal time and temperature of heat treatment for the development of thin film coatings with the most desired grain size and surface adhesion to the Ni-201 substrate.

BIBLIOGRAPHY

1. Allegheny Tech Inc. (2012). *Nickel Technical Data Sheet 2*.
2. Allison, H. W., & Samelson, H. (1958). Diffusion of Aluminum, Magnesium, Silicon, and Zirconium in Nickel. *Journal of Applied Physics* 30, 1419-1424.
3. Ambios Tech., T. (1996). Ambios Technology XP-2 Stylus Profiler Specifications. Santa Cruz, CA, USA.
4. Ashby, M., Shercliff, H., & Cebon, D. (2010). *Materials: Engineering, Science, Processing, and Design*. Canada: Elsevier Ltd.
5. Barkalow, R. H., & Pettit, F. S. (1978). Degradation of Coating Alloys in Simulated Marine Environments. *Naval Research Laboratory*.
6. Barsoum, M. W. (2013). *MAX Phases: Properties of Machinable Ternary Carbides and Nitrides*. Hoboken: Wiley.
7. Birks, N., Meier, G. H., & Pettit, F. S. (2006). *Introduction to the High-Temperature Oxidation of Metals*. New York: Cambridge University Press.
8. Bunshaw, R. F. (1994). *Handbook of Deposition Technologies for Films and Coatings, 2nd Edition*. Noyes Publications.
9. Chen, T. F., Iijima, Y., Hirano, K., & Kiyoshi, Y. (1989). Diffusion of Chromium in Nickel Based Ni-Cr-Fe Alloys. *Journal of Nuclear Materials* 169, 285-290.
10. Chiang, K. T., Pettit, F. S., & Meier, G. H. (1983). *High Temperature Corrosion*. National Society of Corrosion Engineers.
11. Davis, A. G., Boone, D. H., & Levy, A. V. (1986). Erosion of Ceramic Thermal Barrier Coatings. *Wear*, 101-116.
12. Debiaggi, S. B., Decorte, P. M., & Monti, A. M. (1996). Diffusion by Vacancy Mechanism in Ni, Al, and Ni₃Al: Calculation Based on Many-Body Potentials. *Phys. Stat. Sol.* 195, 37-54.
13. Deodeshmukh, V., & Gleeson, B. (2007). Evaluation of the Hot Corrosion Resistance of Commercial β -NiAl and developmental γ' -Ni₃Al + γ -Ni-based Coatings. *Surface & Coatings Technology*, 643-647.
14. Eason, R. (2007). Pulsed Laser Deposition of Thin Films: Applications-Led Growth of Functional Materials. p. 4.

15. Eliaz, N., Shemesh, G., & Latanision, R. M. (2002). Hot Corrosion in Gas Turbine Components. *Engineering Failure Analysis*, 23- 31.
16. Fujiwara, K., & Horita, Z. (2002). Measurement of Intrinsic Diffusion Coefficients of Al and Ni in Ni₃Al Using Ni/NiAl Diffusion Couples. *Acta Materialia* 50, 1571-1579.
17. Fuller, C. R., & Ghate, P. B. (1979). Magnetron Sputtered Aluminum Films for Integrated Circuit Interconnections. *Thin Solid Films*, 64, 25-37.
18. Gill, Z. E. (2014, May 5). A Fundamental Study of Hot Corrosion and Interdiffusion of Chromium, Aluminum, and Silicon Coatings on Nickel 201 Substrate. Bozeman, Montana, United States of America.
19. Gleeson, B. (2013). Environmental and Compositional Effects on Deposit Induced Hot Corrosion: Improving Testing and Extending Component Performance. *Office of Naval Research* (pp. 1-25). Pittsburgh: University of Pittsburgh.
20. Hamdi, M., & Ide-Ektessabi, A. (2003). Preparation of Hydroxyapatite Layer by Ion Beam Assisted Simultaneous Vapor Deposition. *Surface and Coatings Technology*, 163-164, 362-367.
21. Harsha, S. (2006). *Principles of Physical Vapor Deposition of Thin Films*. Elsevier B.V.
22. Himmer, P. (2011). *Montana Microfabrication Facility* . Retrieved from Montana State University, Bozeman Website:
<http://www.mmf.montana.edu/equipment/angstrom-sputter-system>
23. Hofsäss, H. C. (2007). *MAX Phases - Ceramics with Metallic Properties*. Retrieved from Atomic and Nuclear Physics: http://physik2.uni-goettingen.de/research/2_hofs/research/maxphases
24. Holler, F. J., Skoog, D. A., & West, D. M. (1996). *Fundamentals of Analytical Chemistry*. Philadelphia: Saunders College Publication.
25. Kannan, P., & Amirthagadeswaran, K. S. (2013). Failures of High Temperature Critical Components in Combined Cycle Power Plants. *Journal of Failure Analysis and Prevention*, 409-419.
26. Khajavi, M. R., & Shariat, M. H. (2004). Failure of First Stage Gas Turbine Blades. *Engineering Failure Analysis* 11, 589-597.
27. Knittl, Z. (1978). *Optics of Thin Films*. New York: Wiley-Interscience Publications.

28. Koster, W., Watchtelund, E., & Grube, K. (1963). Aluminum- Chromium Binary Alloy Phase Diagram. *Z. Metallkd.*, 393-401.
29. Lee, D. B., Nguyen, T. D., & Park, S. W. (2011). Corrosion of Cr₂AlC in Ar/1%SO₂ Gas Between 900C and 1200C. *Oxidation of Metals*, 313-323.
30. Lee, D. B., Nguyen, T. D., & Park, S. W. (2012). Long Time Oxidation of Cr₂AlC Between 700C and 1000C in Air. *Oxidation of Metals*, 275-287.
31. Li, J. J., Li, M. S., Xiang, H. M., Lu, X. P., & Zhou, Y. C. (2011). Short-term Oxidation Resistance and Degradation of Cr₂AlC Coatings on M38G Superalloy at 900-1100C. *Corrosion Science* 53, 3813-3820.
32. Liang, Y., Guo, C., Li, C., & Du, Z. (2007). Thermodynamic Modeling of the Al - Cr System. *Journal of Alloys and Compounds*, 314-319.
33. Lillerud, K., & Kofstad, P. (1984). Sulphate Induced Hot Corrosion of Nickel. *Oxidation of Metals, Vol. 21*, 252.
34. Lin, Z. J., Li, M. S., Wang, J. Y., & Zhou, Y. C. (2007). High Temperature Oxidation and Hot Corrosion of Cr₂AlC. *Acta Materialia* 55, 6182-6191.
35. Luthra, K., & Shores, D. (1980). *Journal of the Electrochemical Society* 127, 2202.
36. Martin, P. M. (2011). *Introduction of Surface Engineering and Functionally Engineered Materials*. Salem, MA: Scrivener Pub.
37. Matta, R., Mercer, G., & Tuthill, R. (2000). *Power Systems for the 21st Century - "H" Gas Turbine Combined-Cycles*. Schenectady, NY: GE Power Systems.
38. Meetham, G., & Voorde, M. V. (2000). *Materials for High Temperature Engineering Applications*. Berlin: Springer.
39. Murray, J. L. (1998). *Phase Equilibria*.
40. Ohno, T., & Toji, A. (2007). Development of Low Thermal Expansion Nickel Base Superalloy for Steam Turbine Applications. *Energy Materials*, 222-226.
41. Ohring, M. (1992). *Materials Science of Thin Films, 2nd Edition*. London: Academic Press.
42. Ou, X.-M., Sun, Z., Sun, M., & Zou, D.-L. (2008). Hot Corrosion Mechanisms of Ni-Cr Coatings at 650C Under Different Simulated Corrosion Conditions. *Journal of China Univeristy of Mining & Technology* 18, 444-448.

43. Pettit, F. (2011). Hot Corrosion of Metals and Alloys. *Oxid Met* (pp. 1-21). Pittsburgh: University of Pittsburgh.
44. Pruthi, D. D., Anand, M. S., & Agarwala, R. P. (1977). Diffusion of Chromium in Inconel-600. *Journal of Nuclear Material* 64, 206-210.
45. Ramqvist, L., Hamrin, K., Johnsson, G., Fahlman, A., & Nordling, C. (1968). Charge Transfer in Transition Metal Carbides and Related Compounds Studied by ESCA. *Journal of Physics and Chemistry of Solids*, 1835-1847.
46. Rothman, S. J., Nowicki, L. J., & Murch, G. E. (1980). Self-diffusion in Austenitic Fe-Cr-Ni Alloys. *J. Phys. F: Metal Phys.*, 383-398.
47. Saini, A. (2012). High Temperature Materials Increase Efficiency of Gas Power Plants. *Energy Quarterly - Energy Sector Analysis*, 550-551.
48. Sartorius Inc. (2014). *Operating Instructions - Sartorius Expert Series: LE Models*. Retrieved from Sartorius Expert Series Data Weighing Systems: https://www.google.com/url?sa=t&rct=j&q=&esrc=s&source=web&cd=2&cad=rja&uact=8&ved=0CDMQFjAB&url=http%3A%2F%2Fwww.dataweigh.com%2Fshared%2Fpdf.asp%3FUploadID%3D1251%26FileName%3DUser%2520manual&ei=tjgsVJnYIY6sogSgyILQCA&usg=AFQjCNHFROcCSfuHSnj--N4a_ty7d-s
49. Sigma-Aldrich. (2014). *Sigma-Aldrich Materials Science Products*. Retrieved from Physical Vapor Deposition (PVD): <http://www.sigmaaldrich.com/materials-science/material-science-products.html?TablePage=108832720>
50. Sivakumar, R., & Mordike, B. L. (1989). High Temperature Coatings for Gas Turbine Blades: A Review. *Surface and Coatings Technology*, 139-160.
51. Stringer, J. (1977). Hot Corrosion of High Temperature Alloys. *Material Science Annual Review* (pp. 8610 - 8615). England: Department of Metallurgy and Material Sciences.
52. Stuart, R. V. (1983). *Vacuum Technology, Thin Films, and Sputtering*. New York: Academic Press, Inc.
53. Task, M., Gleeson, B., Pettit, F., & Meier, G. (2013). The Effect of Microstructure on the Type II Hot Corrosion of Ni-based MCrAlY Alloys. *Oxidation of Metals Journal*, 125-146.
54. Thompson, D. H. (2013). *Purdue University Department of Chemistry*. Retrieved from Purdue University Website: <http://www.chem.purdue.edu/gchelp/howtosolveit/Solutions/concentrations.html>

55. Tian, W., Wang, P., & Zhang, G. (2006). Synthesis and Thermal and Electrical Properties of Bulk Cr₂AlC. *Scripta Materialia* 54, 841-846.
56. Tschinkel, J. (1972). *Corrosion*. 28: 161.
57. Valenti, M. (2002). Reaching for 60 Percent. *Feature Focus: Advanced Energy Systems*, 35-39.
58. Vargas, J. R., Ulion, N. E., & Goebel, J. A. (1980). Advanced Coating Development for Industrial Utility Gas Turbine Engines. *Thin Solid Films*, 407-413.
59. Walker, M. (2014, July 25). *What is RF Sputtering*. Retrieved from wiseGEEK.org: <http://www.wisegeek.org/what-is-rf-sputtering.htm>
60. Wang, K., Liu, Y., & Fergus, J. W. (2011). Interactions Between SOFC Interconnect Coating Materials and Chromia. *The American Ceramic Society*, 4490-4495.
61. Wang, Q. M., Mykhaylonka, R., Renteria, A. F., Zhang, J. L., Leyens, C., & Kim, K. (2010). Improving the High Temperature Oxidation Resistance of a TiAl Alloy by a Cr₂AlC Coating. *Corrosion Science* 52, 3793-3802.
62. Wang, Q. M., Renteria, A. F., Schroeter, O., Mykhaylonka, R., Leyens, C., Garkas, W., & Baben, M. (2010). Fabrication and Oxidation Behavior of Cr₂AlC Coating on Ti6242 Alloy. *Surface & Coatings Technology* 204, 2343-2352.
63. Yari, M., Larijani, M. M., Afshar, A., Eshghabadi, M., & Shokouhy, A. (2012). Physical Properties of Sputtered Amorphous Carbon Coating. *Journal of Alloys and Compounds*, 135-138.
64. Zhang, S., Li, L., & Kumar, A. (2009). *Materials Characterization Techniques*. Boca raton, FL: Taylor & Francis Group, LLC.
65. Zheng, R. S., & Bu, Q. W. (1990). Erosion of Protective Coatings. *Surface and Coatings Technology*, 875-887.